Isospin-dependent properties of asymmetric nuclear matter in relativistic mean-field models

Lie-Wen Chen,[1,2] Che Ming Ko,[3] and Bao-An Li[4]

[1]*Institute of Theoretical Physics, Shanghai Jiao Tong University, Shanghai 200240, China*
[2]*Center of Theoretical Nuclear Physics, National Laboratory of Heavy Ion Accelerator, Lanzhou 730000, China*
[3]*Cyclotron Institute and Physics Department, Texas A&M University, College Station, Texas 77843-3366, USA*
[4]*Department of Physics, Texas A&M University-Commerce, Commerce, Texas 75429-3011, USA*

(Dated: February 1, 2008)

Using various relativistic mean-field models, including the nonlinear ones with meson field self-interactions, those with density-dependent meson-nucleon couplings, and the point-coupling models without meson fields, we have studied the isospin-dependent bulk and single-particle properties of asymmetric nuclear matter. In particular, we have determined the density dependence of nuclear symmetry energy from these different relativistic mean-field models and compare the results with the constraints recently extracted from analyses of experimental data on isospin diffusion and isotopic scaling in intermediate-energy heavy ion collisions as well as from measured isotopic dependence of the giant monopole resonances in even-A Sn isotopes. Among the 23 parameter sets in the relativistic mean-filed model that are commonly used for nuclear structure studies, only a few are found to give symmetry energies that are consistent with the empirical constraints. We have also studied the nuclear symmetry potential and the isospin-splitting of the nucleon effective mass in isospin asymmetric nuclear matter. We find that both the momentum dependence of the nuclear symmetry potential at fixed baryon density and the isospin-splitting of the nucleon effective mass in neutron-rich nuclear matter depend not only on the nuclear interactions but also on the definition of the nucleon optical potential.

PACS numbers: 21.65.+f, 21.30.Fe, 24.10.Jv

I. INTRODUCTION

Besides the many existing radioactive beam facilities and their upgrades, many more are being constructed or under planning, including the Cooling Storage Ring (CSR) facility at HIRFL in China [1], the Radioactive Ion Beam (RIB) Factory at RIKEN in Japan [2], the FAIR/GSI in Germany [3], SPIRAL2/GANIL in France [4], and the Facility for Rare Isotope Beams (FRIB) in the USA [5]. These new facilities offer the possibility to study the properties of nuclear matter or nuclei under the extreme condition of large isospin asymmetry. As a result, the study of the isospin degree of freedom in nuclear physics has recently attracted much attention. The ultimate goal of such study is to extract information on the isospin dependence of in-medium nuclear effective interactions as well as the equation of state (EOS) of isospin asymmetric nuclear matter, particularly its isospin-dependent term or the density dependence of the nuclear symmetry energy. This knowledge, especially the latter, is important for understanding not only the structure of radioactive nuclei, the reaction dynamics induced by rare isotopes, and the liquid-gas phase transition in asymmetric nuclear matter, but also many critical issues in astrophysics [6, 7, 8, 9, 10, 11, 12, 13]. Unfortunately, the density dependence of the nuclear symmetry energy, especially its behavior at high densities, is largely unknown and is regarded as the most uncertain among all the properties of isospin asymmetric nuclear matter. Although the nuclear symmetry energy at normal nuclear matter density $\rho_0 \approx 0.16$ fm^{-3} is known to be around 30 MeV from the empirical liquid-drop mass formula [14, 15], its values at other densities are poorly known [6, 7]. Various microscopic and phenomenological models, such as the relativistic Dirac-Brueckner-Hartree-Fock (DBHF) [16, 17, 18, 19, 20, 21, 22] and the non-relativistic Brueckner-Hartree-Fock (BHF) [23, 24] approach, the relativistic mean-field (RMF) model based on nucleon-meson interactions [12], and the non-relativistic mean-field model based on Skyrme-like interactions [25, 26, 27, 28, 29, 30, 31], have been used to study the isospin-dependent properties of asymmetric nuclear matter, such as the nuclear symmetry energy, the nuclear symmetry potential, the isospin-splitting of nucleon effective mass, etc., but the predicted results vary widely. In fact, even the sign of the symmetry energy above $3\rho_0$ is uncertain [32]. The theoretical uncertainties are mainly due to the lack of knowledge about the isospin dependence of in-medium nuclear effective interactions and the limitations in the techniques for solving the nuclear many-body problem. As to the incompressibility of asymmetric nuclear matter, it is essentially undetermined [33], even after about 30 years of studies. For comparison, the incompressibility of symmetric nuclear matter at its saturation density ρ_0 has been determined to be 231 ± 5 MeV from the nuclear GMR [34] and the EOS at densities of $2\rho_0 < \rho < 5\rho_0$ has also been constrained by measurements of collective flows in nucleus-nucleus collisions [8].

As a phenomenological approach, the RMF model has achieved great success during the last decade in describing many nuclear phenomena [35, 36, 37, 38, 39, 40, 41,

42]. For example, it provides a novel saturation mechanism for the nuclear matter, an explanation of the strong spin-orbit interaction in finite nuclei, a natural energy dependence of the nucleon optical potential, etc. The RMF approach is generally based on effective interaction Lagrangians that involve nucleon and meson fields. In this approach, a number of parameters are adjusted to fit the properties of many nuclei. As such, these models usually give excellent descriptions of nuclear properties around or below the saturation density.

Since the original Lagrangian proposed by Walecka more than 30 years ago [35], there have been a lot of different treatments, extensions, and applications of the RMF model. The three main versions are the nonlinear models [36, 37, 38, 39], models with density-dependent meson-nucleon couplings [43, 44, 45, 46, 47], and point-coupling models without mesons [48, 49, 50, 51, 52, 53]. For each version of the RMF model, there are also many different parameter sets with their values fitted to the binding energies and charge radii of a large number of nuclei in the periodic table. Including isovector mesons in the effective interaction Lagrangians further allows the RMF model to describe successfully the properties of nuclei far from the β-stability line. With recent developments in constraining the isospin-dependent properties of asymmetric nuclear matter, especially the density dependence of the nuclear symmetry energy, it is of great interest to see to what extend the results from different versions of the RMF model are consistent with these constrains.

In the present work, based on commonly used 23 different parameter sets in three different versions of the RMF model, we carry out a systematic study of the isospin-dependent bulk and single-particle properties of asymmetric nuclear matter. In particular, we study the density dependence of the nuclear symmetry energy from these RMF models and compare the results with the constraints recently extracted from analyses of the isospin diffusion data from heavy-ion collisions based on the isospin and momentum-dependent IBUU04 transport model with in-medium nucleon-nucleon (NN) cross sections [54, 55, 56], the isoscaling analyses of isotope ratios in intermediate energy heavy ion collisions [57], and measured isotopic dependence of the giant monopole resonances (GMR) in even-A Sn isotopes [58]. Among these 23 commonly used interactions in nuclear structure studies, only a few are found to give symmetry energies that are consistent with the empirically extracted one. Furthermore, we study the nuclear symmetry potential and the isospin-splitting of the nucleon effective mass in isospin asymmetric nuclear matter. Our results indicate that the nuclear symmetry potential at fixed baryon density may increase or decrease with increasing nucleon momentum depending on the definition of the nucleon optical potential and the interactions used. This dependence is also seen in the isospin-splitting of the nucleon effective mass in neutron-rich nuclear matter. In addition, the isospin-splitting of the nucleon scalar density in neutron-rich nuclear matter is also studied.

The paper is organized as follows. In Section II, we discuss some isospin-dependent bulk and single-particle properties of asymmetric nuclear matter, such as the nuclear symmetry energy, the nuclear symmetry potential, and the isospin-splitting of nucleon effective mass as well as current experimental and/or empirical constraints on these quantities. The theoretical frameworks for the different versions of RMF models, i.e., the nonlinear RMF models, the models with density-dependent nucleon-meson coupling, and the nonlinear and density-dependent point-coupling models, are briefly reviewed in Section III. Results on the isospin-dependent properties of asymmetric nuclear matter, i.e., the nuclear symmetry energy, the nuclear symmetry potential, and the isospin-splitting of nucleon effective mass and the nucleon scalar densities in neutron-rich nuclear matter, from different versions of RMF models are presented and discussed in Section IV. A summary is then given in Section V. For completeness, the isospin- and momentum-dependent MDI interaction, which will be used as a reference in some cases for comparison, is briefly described in Appendix A.

II. ISOSPIN-DEPENDENT PROPERTIES OF ASYMMETRIC NUCLEAR MATTER

A. Nuclear symmetry energy

The EOS of isospin asymmetric nuclear matter, given by its binding energy per nucleon, can be generally written as

$$E(\rho,\alpha) = E(\rho,\alpha=0) + E_{\rm sym}(\rho)\alpha^2 + O(\alpha^4), \quad (1)$$

where $\rho = \rho_n + \rho_p$ is the baryon density with ρ_n and ρ_p denoting the neutron and proton densities, respectively; $\alpha = (\rho_n - \rho_p)/(\rho_p + \rho_n)$ is the isospin asymmetry; $E(\rho,\alpha = 0)$ is the binding energy per nucleon in symmetric nuclear matter, and

$$E_{\rm sym}(\rho) = \frac{1}{2}\frac{\partial^2 E(\rho,\alpha)}{\partial\alpha^2}|_{\alpha=0} \quad (2)$$

is the nuclear symmetry energy. The absence of odd-order terms in α in Eq. (1) is due to the exchange symmetry between protons and neutrons in nuclear matter when one neglects the Coulomb interaction and assumes the charge symmetry of nuclear forces. The higher-order terms in α are negligible, e.g., the magnitude of the α^4 term at ρ_0 is estimated to be less than 1 MeV [59, 60, 61]. Neglecting the contribution from higher-order terms in Eq. (1) leads to the well-known empirical parabolic law for the EOS of asymmetric nuclear matter, which has been verified by all many-body theories to date, at least for densities up to moderate values. As a good approximation, the density-dependent symmetry energy $E_{\rm sym}(\rho)$ can be extracted from $E_{\rm sym}(\rho) \approx E(\rho,\alpha = 1) - E(\rho,\alpha = 0)$, i.e., the energy change per nucleon when all protons

in the symmetric nuclear matter are converted to neutrons while keeping the total nuclear density fixed. In this sense, the nuclear symmetry energy gives an estimation of the binding energy difference between the pure neutron matter without protons and the symmetric nuclear matter with equal numbers of protons and neutrons. It should be mentioned that the possible presence of the higher-order terms in α at supra-normal densities can significantly modify the proton fraction in β-equilibrium neutron-star matter and the critical density for the direct Urca process which can lead to faster cooling of neutron stars [62, 63].

Around the nuclear matter saturation density ρ_0, the nuclear symmetry energy $E_{\rm sym}(\rho)$ can be expanded to second-order in density as

$$E_{\rm sym}(\rho) = E_{\rm sym}(\rho_0) + \frac{L}{3}\left(\frac{\rho-\rho_0}{\rho_0}\right) + \frac{K_{\rm sym}}{18}\left(\frac{\rho-\rho_0}{\rho_0}\right)^2, \tag{3}$$

where L and $K_{\rm sym}$ are the slope and curvature parameters of the nuclear symmetry energy at ρ_0, i.e.,

$$L = 3\rho_0 \frac{\partial E_{\rm sym}(\rho)}{\partial \rho}|_{\rho=\rho_0}, \tag{4}$$

$$K_{\rm sym} = 9\rho_0^2 \frac{\partial^2 E_{\rm sym}(\rho)}{\partial^2 \rho}|_{\rho=\rho_0}. \tag{5}$$

The L and $K_{\rm sym}$ characterize the density dependence of the nuclear symmetry energy around normal nuclear matter density, and thus carry important information on the properties of nuclear symmetry energy at both high and low densities. In particular, the slope parameter L has been found to correlate linearly with the neutron-skin thickness of heavy nuclei and thus can in principle be determined from measured thickness of the neutron skin of such nuclei [64, 65, 66, 67, 68, 69, 70, 71]. Unfortunately, because of the large uncertainties in the experimental measurements, this has not yet been possible so far.

At the nuclear matter saturation density and around $\alpha = 0$, the isobaric incompressibility of asymmetric nuclear matter can also be expressed to second-order in α as [72, 73]

$$K(\alpha) \approx K_0 + K_{\rm asy}\alpha^2, \tag{6}$$

where K_0 is the incompressibility of symmetric nuclear matter at the nuclear matter saturation density and the isospin-dependent part [74]

$$K_{\rm asy} \approx K_{\rm sym} - 6L \tag{7}$$

characterizes the density dependence of the nuclear symmetry energy. Information on $K_{\rm asy}$ can in principle be extracted experimentally by measuring the GMR in neutron-rich nuclei. Earlier attempts based on this method have given, however, widely different values. For example, a value of $K_{\rm asy} = -320 \pm 180$ MeV with a large uncertainty was obtained in Ref. [75] from a systematic study of the GMR in the isotopic chains of Sn and Sm. In this analysis, the value of K_0 was found to be 300 ± 25 MeV, which is somewhat larger than the commonly accepted value of 230 ± 10 MeV. In a later study, an even less stringent constraint of $-566 \pm 1350 < K_{\rm asy} < 139 \pm 1617$ MeV was extracted from the GMR of finite nuclei, depending on the mass region of nuclei and the number of parameters used in parameterizing the incompressibility of finite nuclei [33]. Most recently, a much stringent constraint of $K_{\rm asy} = -550 \pm 100$ MeV has been obtained in Ref. [58] from measurements of the isotopic dependence of the GMR in even-A Sn isotopes.

Besides studies of nuclear structure, heavy-ion reactions, especially those induced by radioactive beams, also provide a useful means to investigate in terrestrial laboratories the isospin-dependent properties of asymmetric nuclear matter, particularly the density dependence of the nuclear symmetry energy. Indeed, significant progress has recently been made both experimentally and theoretically in extracting the information on the behaviors of nuclear symmetry energy at sub-saturation density from the isospin diffusion data in heavy-ion collisions from the NSCL/MSU [54, 55, 56]. Using the isospin and momentum-dependent IBUU04 transport model with in-medium NN cross sections, the isospin diffusion data were found to be consistent with a density-dependent symmetry energy of $E_{\rm sym}(\rho) \approx 31.6(\rho/\rho_0)^\gamma$ with $\gamma = 0.69 - 1.05$ at subnormal density [55, 56], which has led to the extraction of a value of $L = 88 \pm 25$ MeV for the slope parameter of the nuclear symmetry energy at saturation density and a value of $K_{\rm asy} = -500 \pm 50$ MeV for the isospin-dependent part of the isobaric incompressibility of isospin asymmetric nuclear matter [55, 56, 70]. This has further imposed stringent constraints on both the parameters in the isospin-dependent nuclear effective interactions and the neutron skin thickness of heavy nuclei. Among the 21 sets of Skyrme interactions commonly used in nuclear structure studies, only the 4 sets SIV, SV, G_σ, and R_σ have been found to give symmetry energies that are consistent with above extracted one. Using these Skyrme interactions, the neutron-skin thickness of heavy nuclei calculated within the Hartree-Fock approach is consistent with available experimental data [70, 71] and also that from a relativistic mean-field model based on an accurately calibrated parameter set that reproduces the GMR in ^{90}Zr and ^{208}Pb as well as the isovector giant dipole resonance of ^{208}Pb [76]. The extracted symmetry energy further agrees with the symmetry energy $E_{\rm sym}(\rho) = 31.6(\rho/\rho_0)^{0.69}$ recently obtained from the isoscaling analyses of isotope ratios in intermediate energy heavy ion collisions [57], which gives $L \approx 65$ MeV and $K_{\rm asy} \approx -453$ MeV. The extracted value of $K_{\rm asy} = -500 \pm 50$ MeV from the isospin diffusion data is also consistent with the value $K_{\rm asy} = -550 \pm 100$ MeV obtained from recently measured isotopic dependence of the GMR in even-A Sn isotopes [58]. We note that the GMR only allows us to extract the value of $K_{\rm asy}$ but not that of L. These empirically extracted values for L and $K_{\rm sym}$ represent the best and most stringent phenomenological

constraints available so far on the nuclear symmetry energy at sub-normal densities. Although the behavior of the symmetry energy at high densities is presently largely undetermined, much of this information is expected to be obtained from future high energy radioactive beam facilities.

B. Nuclear symmetry potential

The nuclear symmetry potential refers to the isovector part of the nucleon mean-field potential in isospin asymmetric nuclear matter. Besides the nuclear density, the symmetry potential of a nucleon in nuclear matter also depends on the momentum or energy of the nucleon. The nuclear symmetry potential is different from the nuclear symmetry energy as the latter involves the integration of the isospin-dependent mean-field potential of a nucleon over its momentum. The nuclear symmetry potential is thus a dynamical quantity while the nuclear symmetry energy is a thermodynamic quantity, and both are important for understanding many physics questions in nuclear physics and astrophysics. Various microscopic and phenomenological models have been used to study the symmetry potential [12, 16, 17, 18, 19, 20, 21, 22, 23, 24, 25, 26, 27, 28, 29, 30, 31], and the predicted results vary widely as in the case of the nuclear symmetry energy. In particular, whereas most models predict a decreasing symmetry potential with increasing nucleon momentum albeit at different rates, a few nuclear effective interactions used in some models give an opposite behavior.

The nuclear symmetry potential was originally defined in non-relativistic models. In particular, the nuclear symmetry potential can be evaluated from

$$U_{\rm sym}(\rho,\vec{p}) = \frac{U_n(\rho,\vec{p}) - U_p(\rho,\vec{p})}{2\alpha} \tag{8}$$

where $U_n(\rho,\vec{p})$ and $U_p(\rho,\vec{p})$ represent, respectively, the neutron and proton single-particle or mean-field potentials In relativistic models, the nuclear symmetry potential can be similarly defined by using the non-relativistic reduction of the relativistic single-nucleon potentials. The nuclear symmetry potential in relativistic models therefore depends on the definition of the real part of the non-relativistic optical potential or the nucleon mean-field potential deduced from the relativistic effective interactions, which are characterized by Lorentz covariant nucleon self-energies. In the relativistic mean-field approximation, these self-energies appear in the single-nucleon Dirac equation

$$[\gamma_\mu(i\partial^\mu - \Sigma_\tau^\mu) - (M_\tau + \Sigma_\tau^S)]\psi_\tau = 0, \quad \tau = n,p \tag{9}$$

as the isospin-dependent nucleon vector self-energy Σ_τ^μ and scalar self-energy Σ_τ^S. In the Hartree approximation at the static limit, there are no currents in a nucleus or nuclear matter, and the spatial vector components vanish and only the time-like component of the vector self-energy Σ_τ^0 remains. Furthermore, the nucleon self-energy is an energy-independent real and local quantity in the standard RMF model.

There are different methods to derive the real part of the non-relativistic optical potential based on the Dirac equation with Lorentz covariant nucleon vector and scalar self-energies. The most popular one is the so-called "Schrödinger-equivalent potential" (SEP). From the nucleon scalar self-energy Σ_τ^S and the time-like component of the vector self-energy Σ_τ^0, the "Schrödinger-equivalent potential " is given by [77]:

$$\begin{aligned} U_{{\rm SEP},\tau} &= \Sigma_\tau^S + \frac{1}{2M_\tau}[(\Sigma_\tau^S)^2 - (\Sigma_\tau^0)^2] + \frac{\Sigma_\tau^0}{M_\tau}E_\tau \\ &= \Sigma_\tau^S + \Sigma_\tau^0 + \frac{1}{2M_\tau}[(\Sigma_\tau^S)^2 - (\Sigma_\tau^0)^2] + \frac{\Sigma_\tau^0}{M_\tau}E_{\rm kin}, \end{aligned} \tag{10}$$

where $E_{\rm kin}$ is the kinetic energy of a nucleon, i.e., $E_{\rm kin} = E_\tau - M_\tau$ with E_τ being its total energy. Eq.(10) shows that $U_{{\rm SEP},\tau}$ increases linearly with the nucleon energy E_τ or kinetic energy $E_{\rm kin}$ if the nucleon self-energies are independent of energy. We note that by construction solving the Schrödinger equation with above SEP gives same bound-state energy eigenvalues and elastic phase shifts as the solution of the upper component of the Dirac spinor in the Dirac equation with same nucleon scalar self-energy and time-like component of the vector self-energy [77]. The above SEP thus best represents the real part of the nucleon optical potential in non-relativistic models [20, 78]. The corresponding nuclear symmetry potential is given by

$$U_{\rm sym}^{\rm SEP} = \frac{U_{{\rm SEP},n} - U_{{\rm SEP},p}}{2\alpha}, \tag{11}$$

with α being the isospin asymmetry.

Another popular alternative for deriving the non-relativistic nucleon optical potential in relativistic models is to take it as the difference between the total energy E_τ of a nucleon with momentum $\vec{p}$ in the nuclear medium and its energy at the same momentum in free space [79], i.e.,

$$\begin{aligned} U_{{\rm OPT},\tau} &= E_\tau - \sqrt{\mathbf{p}^2 + M_\tau^2} \\ &= E_\tau - \sqrt{(E_\tau - \Sigma_\tau^0)^2 - \Sigma_\tau^S(2M_\tau + \Sigma_\tau^S)} \end{aligned} \tag{12}$$

In obtaining the last step in above equation, the dispersion relation

$$E_\tau = \Sigma_\tau^0 + \sqrt{\mathbf{p}^2 + (M_\tau + \Sigma_\tau^S)^2} \tag{13}$$

has been used. This definition for the nucleon optical potential has also been extensively used in microscopic DBHF calculations [80] and transport models for heavy-ion collisions [81]. For energy-independent nucleon self-energies, $U_{{\rm OPT},\tau}$ approaches a constant value of Σ_τ^0 when $|\vec{p}| \to \infty$, unlike the linear increase of $U_{{\rm SEP},\tau}$ with the nucleon energy. For $|\vec{p}| = 0$, we have $U_{{\rm OPT},\tau} = \Sigma_\tau^S + \Sigma_\tau^0$

while $U_{\rm SEP,\tau}=\Sigma^S_\tau+\Sigma^0_\tau+(\Sigma^S_\tau+\Sigma^0_\tau)^2/(2M_\tau)$. Therefore, $U_{\rm OPT,\tau}$ displays a more reasonable high energy behavior than $U_{\rm SEP,\tau}$. We note that unlike $U_{\rm SEP,\tau}$, $U_{\rm OPT,\tau}$ does not give the same bound-state energy eigenvalues and elastic phase shifts as the solution of the upper component of the Dirac equation. As in the case of $U_{\rm SEP,\tau}$, the symmetry potential in this approach is defined by

$$U^{\rm OPT}_{\rm sym}=\frac{U_{\rm OPT,n}-U_{\rm OPT,p}}{2\alpha}. \quad (14)$$

In Ref. [82], another optical potential was introduced based on the second-order Dirac (SOD) equation, and it corresponds to multiplying Eq.(10) by the factor M_τ/E_τ, i.e.,

$$\begin{aligned} U_{\rm SOD,\tau} &= [\Sigma^S_\tau+\frac{1}{2M_\tau}[(\Sigma^S_\tau)^2-(\Sigma^0_\tau)^2]+\frac{\Sigma^0_\tau}{M_\tau}E_\tau]\frac{M_\tau}{E_\tau} \\ &= \Sigma^0_\tau+\frac{M_\tau}{E_\tau}\Sigma^S_\tau+\frac{1}{2E_\tau}[(\Sigma^S_\tau)^2-(\Sigma^0_\tau)^2]. \quad (15)\end{aligned}$$

For energy-independent nucleon self-energies, $U_{\rm SOD,\tau}$ has the same asymptotical value of Σ^0_τ as $U_{\rm OPT,\tau}$ when $|\vec{p}|\to\infty$. For $|\vec{p}|=0$, we have $U_{\rm SOD,\tau}=\Sigma^0_\tau+\frac{M_\tau}{\Sigma^S_\tau+\Sigma^0_\tau+M_\tau}\Sigma^S_\tau+\frac{1}{2(\Sigma^S_\tau+\Sigma^0_\tau+M_\tau)}[(\Sigma^S_\tau)^2-(\Sigma^0_\tau)^2]$. The symmetry potential based on the optical potential of Eq. (15) is given by

$$U^{\rm SOD}_{\rm sym}=\frac{U_{\rm SOD,n}-U_{\rm SOD,p}}{2\alpha}. \quad (16)$$

Above discussions thus show that the optical potentials defined in Eqs. (12) and (15) have similar high energy behaviors, but they may be very different from that defined in Eq. (10). If we assume that $\Sigma^S_\tau+\Sigma^0_\tau\ll M_\tau$ and $\left|\Sigma^S_\tau\right|\approx\left|\Sigma^0_\tau\right|$, which has been shown to be generally valid in the RMF model even at higher baryon densities, we have, however, $U_{\rm SEP,\tau}\approx U_{\rm SOD,\tau}\approx U_{\rm OPT,\tau}=\Sigma^S_\tau+\Sigma^0_\tau$ at low momenta ($|\vec{p}|\approx 0$), indicating that above three definitions for the optical potential in the RMF model behave similarly at low energies. However, it should be stressed that, among the three optical potentials defined above, only $U_{\rm SEP,\tau}$ is obtained from a well-defined theoretical procedure and is Schrödinger-equivalent while $U_{\rm OPT,\tau}$ and $U_{\rm SOD,\tau}$ are used here for heuristic reasons as they are of practical interest in microscopic DBHF calculations, transport models for heavy-ion collisions, and Dirac phenomenology.

Empirically, a systematic analysis of a large number of nucleon-nucleus scattering experiments and (p,n) charge-exchange reactions at beam energies up to about 100 MeV has shown that the data can be very well described by the parametrization $U_{\rm sym}=a-bE_{\rm kin}$ with $a\approx 22-34$ MeV and $b\approx 0.1-0.2$ [83, 84, 85, 86]. Although the uncertainties in both parameters a and b are large, the nuclear symmetry potential at nuclear matter saturation density, i.e., the Lane potential $U_{\rm Lane}$ [87], clearly decreases approximately linearly with increasing beam energy $E_{\rm kin}$. This provides a stringent constraint on the low energy behavior of the nuclear symmetry potential at saturation density. As we will see in the following, although the predicted energy dependence of nuclear symmetry potential at low energy from the RMF models does not agree with the empirical Lane potential, it is consistent with results from microscopic DBHF [17], the extended BHF with 3-body forces [24], and chiral perturbation theory calculations [88], which give a Lane potential that also stays as a constant or increases slightly with momentum for nucleons with momenta less than about $250-300$ MeV/c or with kinetic energies $E_{\rm kin}<0$ but decreases with momentum when the momentum is larger than about $250-300$ MeV/c.

Recently, the high energy behavior of the nuclear symmetry potential has been studied in the relativistic impulse (t-ρ) approximation based on the empirical NN scattering amplitude [89]. The results indicate that the nuclear symmetry potential derived from the Schrödinger-equivalent potential at a fixed density becomes almost constant when the nucleon kinetic energy is greater than about 500 MeV, independent of the parameters used in the analysis. It is further shown that for such high energy nucleons the nuclear symmetry potential is slightly negative at baryon densities below about $\rho=0.22$ fm^{-3} and then increases almost linearly to positive values at high densities. These results provide important constraints on the high energy behavior of the nuclear symmetry potential in asymmetric nuclear matter. Furthermore, with the Love-Franey NN scattering amplitude developed by Murdock and Horowitz [90, 91], the intermediate-energy ($100\leq E_{kin}\leq 400$ MeV) behavior of the nuclear symmetry potential constructed from the Schrödinger-equivalent potential in isospin asymmetric nuclear matter has also been investigated recently [92]. It shows that the nuclear symmetry potential at fixed baryon density decreases with increasing nucleon energy. In particular, the nuclear symmetry potential at saturation density changes from positive to negative values at nucleon kinetic energy of about 200 MeV. Such an energy and density dependence of the nuclear symmetry potential is consistent with those from the isospin- and momentum-dependent MDI interaction with $x=0$ (see Appendix A for details on this interaction). These results thus provide an important consistency check for the energy/momentum dependence of the nuclear symmetry potential in asymmetric nuclear matter, particularly the MDI interaction with $x=0$. On the other other, the low energy behavior of the nuclear symmetry potential at densities away from normal nuclear density is presently not known empirically. Experimental determination of both the density and momentum dependence of the nuclear symmetry potential is thus of great interest, and heavy-ion reactions with radioactive beams provides a unique tool to extract this information in terrestrial laboratories.

C. Nucleon effective mass

Many different definitions for the nucleon effective mass can be found in the literature [20, 78]. In the present work, we mainly focus on the following three effective masses: the Dirac mass $M^*_{\rm Dirac}$ (also denoted as M^* in the present work), the Landau mass $M^*_{\rm Landau}$, and the Lorentz mass $M^*_{\rm Lorentz}$. The Dirac mass $M^*_{\rm Dirac}$ is defined through the nucleon scalar self-energy in the Dirac equation, i.e.,

$$M^*_{{\rm Dirac},\tau} = M_\tau + \Sigma^S_\tau. \quad (17)$$

It is directly related to the spin-orbit potential in finite nuclei and is thus a genuine relativistic quantity without non-relativistic correspondence. We note that the difference between the nucleon vector and scalar self-energies determines the spin-orbit potential, whereas their sum defines the effective single-nucleon potential and is constrained by the nuclear matter binding energy at saturation density. From the energy spacings between spin-orbit partner states in finite nuclei, the constraint $0.55\ M \leq M^*_{\rm Dirac} \leq 0.6\ M$ has been obtained on the value of the Dirac mass [93, 94].

The Landau mass $M^*_{\rm Landau}$ is defined as $M^*_{{\rm Landau},\tau} = p\frac{dp}{dE_\tau}$ in terms of the single-particle density of state dE_τ/dp at energy E_τ and thus characterizes the momentum dependence of the single-particle potential. In the relativistic model, it is given by [93]

$$M^*_{{\rm Landau},\tau} = (E_\tau - \Sigma^0_\tau)(1 - \frac{d\Sigma^0_\tau}{dE_\tau}) - (M_\tau + \Sigma^S_\tau)\frac{d\Sigma^S_\tau}{dE_\tau} \quad (18)$$

Since dp/dE_τ is in principle measurable, the Landau mass from the relativistic model should have a comparable value as that in the non-relativistic model. Empirically, based on non-relativistic effective interactions such as the Skyrme-type interactions, calculations of the ground-state properties and the excitation energies of quadrupole giant resonances have shown that a realistic choice for the nucleon Landau mass is $M^*_{\rm Landau}/M = 0.8 \pm 0.1$ [94, 95, 96, 97]. The smaller Landau mass than that of nucleon free mass would lead to a smaller level density at the Fermi energy and much spreaded single-particle levels in finite nuclei [93].

The Lorentz mass $M^*_{\rm Lorentz}$ characterizes the energy dependence of the Schrödinger-equivalent Potential $U_{{\rm SEP},\tau}$ in the relativistic model and is defined as [78]

$$\begin{aligned} M^*_{{\rm Lorentz},\tau} &= M_\tau(1 - \frac{dU_{{\rm SEP},\tau}}{dE_\tau}) \\ &= (E_\tau - \Sigma^0_\tau)(1 - \frac{d\Sigma^0_\tau}{dE_\tau}) \\ &\quad -(M_\tau + \Sigma^S_\tau)\frac{d\Sigma^S_\tau}{dE_\tau} + M_\tau - E_\tau \\ &= M^*_{{\rm Landau},\tau} + M_\tau - E_\tau. \end{aligned} \quad (19)$$

It has been argued in Ref. [78] that it is the Lorentz mass $M^*_{\rm Lorentz}$ that should be compared with the usual non-relativistic nucleon effective mass extracted from analyses carried out in the framework of non-relativistic optical and shell models. It can be easily seen that in the non-relativistic approximation ($E_\tau \approx M_\tau$), the Lorentz mass $M^*_{\rm Lorentz}$ reduces to the Landau mass $M^*_{\rm Landau}$.

In relativistic models, the nucleon effective mass has sometimes also been introduced via the energy dependence of the optical potential in Eq. (12) and the second-order Dirac optical potential in Eq. (15), i.e.,

$$\begin{aligned} M^*_{{\rm OPT},\tau} &= M_\tau(1 - \frac{dU_{{\rm OPT},\tau}}{dE_\tau}) \\ &= M_\tau \frac{(E_\tau - \Sigma^0_\tau)(1 - \frac{d\Sigma^0_\tau}{dE_\tau}) + (M_\tau - \Sigma^S_\tau)\frac{d\Sigma^S_\tau}{dE_\tau}}{\sqrt{(E_\tau - \Sigma^0_\tau)^2 - \Sigma^S_\tau(2M_\tau + \Sigma^S_\tau)}} \\ &= M_\tau \frac{M^*_{{\rm Landau},\tau}}{\sqrt{(E_\tau - \Sigma^0_\tau)^2 - \Sigma^S_\tau(2M_\tau + \Sigma^S_\tau)}} \end{aligned} \quad (20)$$

and

$$\begin{aligned} & M^*_{{\rm SOD},\tau} \\ &= M_\tau(1 - \frac{dU_{{\rm SOD},\tau}}{dE_\tau}) \\ &= M_\tau[\frac{M^*_{{\rm Landau},\tau}}{E_\tau} \\ &\quad + \frac{(M_\tau + \Sigma^S_\tau)^2 - (E_\tau - \Sigma^0_\tau)^2 + E^2_\tau - M^2_\tau}{2E^2_\tau}], \end{aligned} \quad (21)$$

respectively.

The isospin-splitting of nucleon effective mass in asymmetric nuclear matter, i.e., the difference between the neutron and proton effective masses is currently not known empirically [98]. Previous theoretical investigations have indicated that most RMF calculations with the isovector δ meson predict $M^*_{{\rm Dirac},n} < M^*_{{\rm Dirac},p}$ while in the microscopic DBHF approach, $M^*_{{\rm Dirac},n}$ can be larger or smaller than $M^*_{{\rm Dirac},p}$ depending on the approximation schemes and methods used for determining the Lorentz and isovector structure of the nucleon self-energy [20]. For the nucleon Lorentz mass, the microscopic DBHF or BHF approach and most non-relativistic Skyrme-Hartree-Fock calculations predict $M^*_{{\rm Lorentz},n} > M^*_{{\rm Lorentz},p}$, while most RMF and a few Skyrme-Hartree-Fock calculations give opposite predictions.

III. RELATIVISTIC MEAN-FIELD MODELS

For completeness, we briefly introduce in the following the main ingredients in the nonlinear RMF model, the density-dependent RMF model, the nonlinear point-coupling RMF model, and the density-dependent point-coupling RMF model. We neglect the electromagnetic field in the following since in the present work we are interested in the properties of the infinite nuclear matter. Furthermore, besides the mean-field approximation in which operators of meson fields are replaced by their expectation values (the fields are thus treated as classical c-numbers), we also use the non-sea approximation

which neglects the effect due to negative energy states in the Dirac sea.

A. The nonlinear RMF model

1. Lagrangian density

The Lagrangian density in the nonlinear RMF model generally includes the nucleon field ψ, the isoscalar-scalar meson field σ, the isoscalar-vector meson field ω, the isovector-vector meson field $\vec{\rho}$, and the isovector-scalar meson field δ, i.e.,

$$\begin{aligned}\mathcal{L}_{\rm NL} &= \bar{\psi}\left[\gamma_\mu(i\partial^\mu - g_\omega\omega^\mu) - (M - g_\sigma\sigma)\right]\psi \\ &+\frac{1}{2}(\partial_\mu\sigma\partial^\mu\sigma - m_\sigma^2\sigma^2) - \frac{1}{4}\omega_{\mu\nu}\omega^{\mu\nu} + \frac{1}{2}m_\omega^2\omega_\mu\omega^\mu \\ &-\frac{1}{3}b_\sigma M(g_\sigma\sigma)^3 - \frac{1}{4}c_\sigma\ (g_\sigma\sigma)^4 + \frac{1}{4}c_\omega(g_\omega^2\omega_\mu\omega^\mu)^2 \\ &+\frac{1}{2}(\partial_\mu\vec{\delta}\cdot\partial^\mu\vec{\delta} - m_\delta^2\vec{\delta}^2) + \frac{1}{2}m_\rho^2\vec{\rho}_\mu\cdot\vec{\rho}^\mu - \frac{1}{4}\vec{\rho}_{\mu\nu}\cdot\vec{\rho}^{\mu\nu} \\ &+\frac{1}{2}(g_\rho^2\vec{\rho}_\mu\cdot\vec{\rho}^\mu)(\Lambda_S g_\sigma^2\sigma^2 + \Lambda_V g_\omega^2\omega_\mu\omega^\mu) \\ &-g_\rho\vec{\rho}_\mu\cdot\bar{\psi}\gamma^\mu\vec{\tau}\psi + g_\delta\vec{\delta}\cdot\bar{\psi}\vec{\tau}\psi\ , \end{aligned} \tag{22}$$

where the antisymmetric field tensors $\omega_{\mu\nu}$ and $\vec{\rho}_{\mu\nu}$ are given by $\omega_{\mu\nu} \equiv \partial_\nu\omega_\mu - \partial_\mu\omega_\nu$ and $\vec{\rho}_{\mu\nu} \equiv \partial_\nu\vec{\rho}_\mu - \partial_\mu\vec{\rho}_\nu$, respectively, and other symbols have their usual meanings. Also, vectors in isospin space are denoted by arrows. This model also contains cross interactions between the isovector meson ρ and isoscalar σ and ω mesons through the cross-coupling constants Λ_S and Λ_V [66, 99]. In addition, we include the isovector-scalar channel (δ meson) which is important for the saturation of asymmetric nuclear matter and has also been shown to be an important degree of freedom in describing the properties of asymmetric nuclear matter [100, 101]. The above Lagrangian density is quite general and allows us to use most of presently popular parameter sets in the nonlinear RMF model.

2. Equation of motion and nucleon self-energies

From the standard Euler-Lagrange formalism, we can deduce from the Lagrangian density equations of motion for the nucleon and meson fields. The resulting Dirac equation for the nucleon field is

$$\left[\gamma_\mu(i\partial^\mu - \Sigma_\tau^\mu) - (M + \Sigma_\tau^S)\right]\psi = 0\ , \tag{23}$$

with the following nucleon scalar and vector self-energies:

$$\Sigma_\tau^S = -g_\sigma\sigma - g_\delta\vec{\delta}\cdot\vec{\tau}, \tag{24}$$

$$\Sigma_\tau^\mu = g_\omega\omega^\mu + g_\rho\vec{\rho}^\mu\cdot\vec{\tau}. \tag{25}$$

For the isoscalar meson fields σ and ω, they are described by the Klein-Gordon and Proca equations, respectively, i.e.,

$$\begin{aligned}(\partial_\mu\partial^\mu + m_\sigma^2)\sigma &= g_\sigma[\bar{\psi}\psi - b_\sigma M(g_\sigma\sigma)^2 - c_\sigma(g_\sigma\sigma)^3 \\ &\quad +\Lambda_S(g_\sigma\sigma)g_\rho^2\vec{\rho}_\mu\cdot\vec{\rho}^\mu]\ , \end{aligned} \tag{26}$$

$$\begin{aligned}\partial_\mu\omega^{\mu\nu} + m_\omega^2\omega^\nu &= g_\omega[\bar{\psi}\gamma^\nu\psi - c_\omega g_\omega^3(\omega_\mu\omega^\mu\omega^\nu) \\ &\quad -\Lambda_V g_\rho^2\vec{\rho}_\mu\cdot\vec{\rho}^\mu g_\omega\omega^\nu]\ . \end{aligned} \tag{27}$$

Analogous equations for the isovector δ and ρ meson fields are

$$(\partial_\mu\partial^\mu + m_\delta^2)\vec{\delta} = g_\delta\bar{\psi}\vec{\tau}\psi, \tag{28}$$

$$\begin{aligned}\partial_\mu\vec{\rho}^{\mu\nu} + m_\rho^2\vec{\rho}^\nu &= g_\rho[\bar{\psi}\gamma^\nu\vec{\tau}\psi - \Lambda_S(g_\rho\vec{\rho}^\nu)(g_\sigma\sigma)^2 \\ &\quad -\Lambda_V(g_\rho\vec{\rho}^\nu)g_\omega^2\omega_\mu\omega^\mu]. \end{aligned} \tag{29}$$

For a static, homogenous infinite nuclear matter, all derivative terms drop out and the expectation values of space-like components of vector fields vanish (only zero components $\vec{\rho}_0$ and ω_0 survive) due to translational invariance and rotational symmetry of the nuclear matter. In addition, only the third component of isovector fields ($\delta^{(3)}$ and $\rho^{(3)}$) needs to be taken into consideration due to the rotational invariance around the third axis in the isospin space. In the mean-field approximation, meson fields are replaced by their expectation values, i.e., $\sigma \to \bar{\sigma}$, $\omega_\mu \to \bar{\omega}_0$, $\vec{\delta} \to \bar{\delta}^{(3)}$, and $\vec{\rho}_\mu \to \bar{\rho}_0^{(3)}$, and the meson field equations are reduced to

$$\begin{aligned}m_\sigma^2\bar{\sigma} &= g_\sigma[\rho_S - b_\sigma M(g_\sigma\bar{\sigma})^2 - c_\sigma(g_\sigma\bar{\sigma})^3 \\ &\quad +\Lambda_S(g_\sigma\bar{\sigma})(g_\rho\bar{\rho}_0^{(3)})^2], \end{aligned} \tag{30}$$

$$\begin{aligned}m_\omega^2\bar{\omega}_0 &= g_\omega[\rho_B - c_\omega(g_\omega\bar{\omega}_0)^3 \\ &\quad -\Lambda(g_\omega\bar{\omega}_0)(g_\rho\bar{\rho}_0^{(3)})^2], \end{aligned} \tag{31}$$

$$m_\delta^2\bar{\delta}^{(3)} = g_\delta(\rho_{S,p} - \rho_{S,n}). \tag{32}$$

$$\begin{aligned}m_\rho^2\bar{\rho}_0^{(3)} &= g_\rho[\rho_{B,p} - \rho_{B,n} - \Lambda_S(g_\rho\bar{\rho}_0^{(3)})(g_\sigma\sigma)^2 \\ &\quad -\Lambda_V(g_\rho\bar{\rho}_0^{(3)})(g_\omega\bar{\omega}_0)^2]. \end{aligned} \tag{33}$$

In the above, the nucleon scalar density ρ_S is defined as

$$\rho_S = \left\langle\bar{\psi}\psi\right\rangle = \rho_{S,p} + \rho_{S,n}\ , \tag{34}$$

with the proton (p) and neutron (n) scalar densities given by

$$\begin{aligned}\rho_{S,i} &= \frac{2}{(2\pi)^3}\int_0^{k_F^i} d^3k\,\frac{M_i^*}{\sqrt{\vec{k}^2 + (M_i^*)^2}} \\ &= \frac{M_i^*}{2\pi^2}\left[k_F^i\tilde{E}_F^i - (M_i^*)^2\ln\frac{k_F^i + \tilde{E}_F^i}{M_i^*}\right], i = p, n \end{aligned} \tag{35}$$

where

$$\tilde{E}_F^i = \sqrt{(k_F^i)^2 + (M_i^*)^2}, \tag{36}$$

with M_p^* and M_n^* denoting the proton and neutron Dirac masses, respectively, i.e.,

$$M_p^* = M - g_\sigma\bar{\sigma} - g_\delta\bar{\delta}^{(3)},\ M_n^* = M - g_\sigma\bar{\sigma} + g_\delta\bar{\delta}^{(3)}. \tag{37}$$

The nucleon scalar and vector self-energies are then given by

$$\Sigma_\tau^S = -g_\sigma\bar{\sigma} - g_\delta\bar{\delta}^{(3)}\tau_3, \quad (38)$$

$$\Sigma_\tau^0 = g_\omega\bar{\omega}_0 + g_\rho\bar{\rho}_0^{(3)}\tau_3, \quad (39)$$

with $\tau_3 = 1$ and -1 for protons and neutrons, respectively.

3. Nuclear matter equation of state

The set of coupled equations for the nucleon and meson fields can be solved self-consistently using the iteration method, and the properties of the nuclear matter can then be obtained from these fields. From the resulting energy-momentum tensor, we can calculate the energy density ϵ and pressure P of asymmetric nuclear matter, and the results are given by

$$\begin{aligned}\epsilon &= \epsilon_{kin}^n + \epsilon_{kin}^p \\ &+\frac{1}{2}\left[m_\sigma^2\bar{\sigma}^2 + m_\omega^2\bar{\omega}_0^2 + m_\delta^2\bar{\delta}^{(3)2} + m_\rho^2\bar{\rho}_0^{(3)2}\right] \\ &+\frac{1}{3}b_\sigma M(g_\sigma\bar{\sigma})^3 + \frac{1}{4}c_\sigma(g_\sigma\bar{\sigma})^4 + \frac{3}{4}c_\omega(g_\omega\bar{\omega}_0)^4 \\ &+\frac{1}{2}(g_\rho\bar{\rho}_0^{(3)})^2[\Lambda_S(g_\sigma\bar{\sigma})^2 + 3\Lambda_V(g_\omega\bar{\omega}_0)^2] \quad (40)\end{aligned}$$

and

$$\begin{aligned}P &= P_{kin}^n + P_{kin}^p \\ &-\frac{1}{2}\left[m_\sigma^2\bar{\sigma}^2 - m_\omega^2\bar{\omega}_0^2 + m_\delta^2\bar{\delta}^{(3)2} - m_\rho^2\bar{\rho}_0^{(3)2}\right] \\ &-\frac{1}{3}b_\sigma M(g_\sigma\bar{\sigma})^3 - \frac{1}{4}c_\sigma(g_\sigma\bar{\sigma})^4 + \frac{1}{4}c_\omega(g_\omega\bar{\omega}_0)^4 \\ &+\frac{1}{2}(g_\rho\bar{\rho}_0^{(3)})^2[\Lambda_S(g_\sigma\bar{\sigma})^2 + \Lambda_V(g_\omega\bar{\omega}_0)^2]. \quad (41)\end{aligned}$$

In the above, ϵ_{kin}^i and P_{kin}^i are, respectively, the kinetic contributions to the energy densities and pressure of protons and neutrons in nuclear matter, and they are given by

$$\begin{aligned}\epsilon_{kin}^i &= \frac{2}{(2\pi)^3}\int_0^{k_F^i} d^3k\sqrt{\vec{k}^2 + (M_i^*)^2} \\ &= \frac{1}{4}[3\tilde{E}_F^i\rho_{B,i} + M_i^*\rho_{S,i}], \quad i = p, n, \quad (42)\end{aligned}$$

and

$$\begin{aligned}P_{kin}^i &= \frac{2}{3(2\pi)^3}\int_0^{k_F^i} d^3k\frac{\vec{k}^2}{\sqrt{\vec{k}^2 + (M_i^*)^2}} \\ &= \frac{1}{4}[\tilde{E}_F^i\rho_{B,i} - M_i^*\rho_{S,i}], \quad i = p, n. \quad (43)\end{aligned}$$

The binding energy per nucleon can be obtained from the energy density via

$$E = \frac{\epsilon}{\rho_B} - M,$$

while the symmetry energy is given by

$$\begin{aligned}E_{\rm sym}(\rho_B) &= \frac{k_F^2}{6\tilde{E}_F} + \frac{1}{2}\left(\frac{g_\rho}{m_\rho^*}\right)^2\rho_B - \frac{1}{2}\left(\frac{g_\delta}{m_\delta}\right)^2 \\ &\times\frac{M^{*2}\rho_B}{\tilde{E}_F^2[1 + \left(\frac{g_\delta}{m_\delta}\right)^2 A(k_F, M^*)]}, \quad (44)\end{aligned}$$

with the effective ρ-meson mass given by [66]

$$m_\rho^{*2} = m_\rho^2 + g_\rho^2[\Lambda_S(g_\sigma\bar{\sigma})^2 + \Lambda_V(g_\omega\bar{\omega}_0)^2] \quad (45)$$

and

$$\begin{aligned}A(k_F, M^*) &= \frac{4}{(2\pi)^3}\int_0^{k_F} d^3k\frac{\vec{k}^2}{\left(\vec{k}^2 + (M^*)^2\right)^{3/2}} \\ &= 3\left(\frac{\rho_S}{M^*} - \frac{\rho_B}{\tilde{E}_F}\right), \quad (46)\end{aligned}$$

where $\tilde{E}_F = \sqrt{k_F^2 + M^{*2}}$ and M^* is the nucleon Dirac mass in symmetric nuclear matter.

B. The density-dependent RMF model

1. Lagrangian density

In the density-dependent RMF model, instead of introducing terms involving self-interactions of the scalar meson field and cross-interactions of meson fields as in the nonlinear RMF model, the coupling constants are density dependent. The Lagrangian density in this model is generally written as

$$\begin{aligned}\mathcal{L}_{\rm DD} &= \bar{\psi}[\gamma_\mu(i\partial^\mu - \Gamma_\omega\omega^\mu - \Gamma_\rho\vec{\rho}^\mu\cdot\vec{\tau}) \\ &-(M - \Gamma_\sigma\sigma - \Gamma_\delta\vec{\delta}\cdot\vec{\tau})]\psi \\ &+\frac{1}{2}(\partial_\mu\sigma\partial^\mu\sigma - m_s^2\sigma^2) + \frac{1}{2}(\partial_\mu\vec{\delta}\cdot\partial^\mu\vec{\delta} - m_\delta^2\vec{\delta}^2) \\ &-\frac{1}{4}\omega_{\mu\nu}\omega^{\mu\nu} + \frac{1}{2}m_\omega^2\omega_\mu\omega^\mu \\ &-\frac{1}{4}\vec{\rho}_{\mu\nu}\cdot\vec{\rho}^{\mu\nu} + \frac{1}{2}m_\rho^2\vec{\rho}_\mu\cdot\vec{\rho}^\mu \quad (47)\end{aligned}$$

The symbols used in above equation have their usual meanings as in Eq.(22) but the coupling constants Γ_σ, Γ_ω, Γ_δ and Γ_ρ now depend on the (baryon) density, which are usually parametrized as

$$\Gamma_i(\rho) = \Gamma_i(\rho_{sat})h_i(x), \quad x = \rho/\rho_{sat}, \quad (48)$$

with

$$h_i(x) = a_i\frac{1 + b_i(x + d_i)^2}{1 + c_i(x + e_i)^2}, \quad i = \sigma, \omega, \delta, \rho, \quad (49)$$

and ρ_{sat} being the saturation density of symmetric nuclear matter. In some parameter sets,

$$h_\rho(x) = \exp[-a_\rho(x - 1)] \quad (50)$$

is used for the ρ meson.

2. Equation of motion and nucleon self-energies

Since the coupling constants in the density-dependent RMF model depend on the baryon fields $\bar{\psi}$ and ψ through the density, additional terms besides the usual ones in the nonlinear RMF model appear in the field equations of motion when the partial derivatives of $\mathcal{L}_{\rm DD}$ are carried out with respect to the fields $\bar{\psi}$ and ψ in the Euler-Lagrange equations. The resulting Dirac equation for the nucleon field now reads:

$$\left[\gamma_\mu(i\partial^\mu - \Sigma_\tau^\mu) - (M + \Sigma_\tau^S)\right]\psi = 0, \tag{51}$$

with the following nucleon scalar and vector self-energies:

$$\begin{aligned}\Sigma_\tau^S &= -\Gamma_\sigma\sigma - \Gamma_\delta\vec{\delta}\cdot\vec{\tau}, &(52)\\ \Sigma_\tau^\mu &= \Gamma_\omega\omega^\mu + \Gamma_\rho\vec{\rho}^\mu\cdot\vec{\tau} + \Sigma^{\mu(R)}. &(53)\end{aligned}$$

The new term $\Sigma^{\mu(R)}$ in the vector self-energy, which is called the *rearrangement* self-energy [43, 44], is given by

$$\begin{aligned}\Sigma^{\mu(R)} &= \frac{j^\mu}{\rho}\Big(\frac{\partial\Gamma_\omega}{\partial\rho}\bar{\psi}\gamma_\nu\psi\omega^\nu + \frac{\partial\Gamma_\rho}{\partial\rho}\bar{\psi}\vec{\tau}\gamma^\nu\psi\cdot\vec{\rho}_\nu\\ &\quad -\frac{\partial\Gamma_\sigma}{\partial\rho}\bar{\psi}\psi\sigma - \frac{\partial\Gamma_\delta}{\partial\rho}\bar{\psi}\vec{\tau}\psi\vec{\delta}\Big)\ , \end{aligned}\tag{54}$$

with $j^\mu = \bar{\psi}\gamma^\mu\psi$. The rearrangement self-energy plays an essential role in the applications of the theory since it guarantees both the thermodynamical consistency and the energy-momentum conservation [43, 44].

For the meson fields, the equations of motion are

$$\begin{aligned}(\partial_\mu\partial^\mu + m_\sigma^2)\sigma &= \Gamma_\sigma\bar{\psi}\psi, &(55)\\ \partial_\nu\omega^{\mu\nu} + m_\omega^2\omega^\mu &= \Gamma_\omega\bar{\psi}\gamma^\mu\psi, &(56)\\ (\partial_\mu\partial^\mu + m_\delta^2)\vec{\delta} &= \Gamma_\delta\bar{\psi}\vec{\tau}\psi, &(57)\\ \partial_\nu\vec{\rho}^{\mu\nu} + m_\rho^2\vec{\rho}^\mu &= \Gamma_\rho\bar{\psi}\vec{\tau}\gamma^\mu\psi. &(58)\end{aligned}$$

In the static case for an infinite nuclear matter, the meson equations of motion become

$$\begin{aligned}m_\sigma^2\bar{\sigma} &= \Gamma_\sigma\rho_S, &(59)\\ m_\omega^2\bar{\omega}_0 &= \Gamma_\omega\rho_B, &(60)\\ m_\rho^2\bar{\rho}_0^{(3)} &= \Gamma_\rho(\rho_p - \rho_n), &(61)\\ m_\delta^2\bar{\delta}^{(3)} &= \Gamma_\delta(\rho_{S,p} - \rho_{S,n}), &(62)\end{aligned}$$

so the nucleon scalar and vector self-energies are

$$\begin{aligned}\Sigma_\tau^S &= -\Gamma_\sigma\bar{\sigma} - \Gamma_\delta\bar{\delta}^{(3)}\tau_3, &(63)\\ \Sigma_\tau^0 &= \Gamma_\omega\bar{\omega}_0 + \Gamma_\rho\bar{\rho}_0^{(3)}\tau_3 + \Sigma^{0(R)}, &(64)\end{aligned}$$

with

$$\begin{aligned}\Sigma^{0(R)} &= \frac{\partial\Gamma_\omega}{\partial\rho}\bar{\omega}_0\rho_B + \frac{\partial\Gamma_\rho}{\partial\rho}\bar{\rho}_0^{(3)}(\rho_p - \rho_n)\\ &\quad -\frac{\partial\Gamma_\sigma}{\partial\rho}\bar{\sigma}\rho_S - \frac{\partial\Gamma_\delta}{\partial\rho}\bar{\delta}^{(3)}(\rho_{S,p} - \rho_{S,n}).\end{aligned}\tag{65}$$

3. Nuclear matter equation of state

From the energy-momentum tensor, the energy density and pressure of nuclear matter can be derived, and they are given by

$$\begin{aligned}\epsilon &= \epsilon_{kin}^n + \epsilon_{kin}^p\\ &\quad +\frac{1}{2}\left[m_\sigma^2\bar{\sigma}^2 + m_\omega^2\bar{\omega}_0^2 + m_\delta^2\bar{\delta}^{(3)2} + m_\rho^2\bar{\rho}_0^{(3)2}\right]\end{aligned}\tag{66}$$

and

$$\begin{aligned}P &= P_{kin}^n + P_{kin}^p + \rho_B\Sigma^{0(R)}\\ &\quad -\frac{1}{2}\left[m_\sigma^2\bar{\sigma}^2 - m_\omega^2\bar{\omega}_0^2 + m_\delta^2\bar{\delta}^{(3)2} - m_\rho^2\bar{\rho}_0^{(3)2}\right].\end{aligned}\tag{67}$$

It is seen that the rearrangement self-energy does not affect the energy density but contributes explicitly to the pressure. Furthermore, the symmetry energy can be written as

$$\begin{aligned}E_{\rm sym}(\rho_B) &= \frac{k_F^2}{6\tilde{E}_F} + \frac{1}{2}\left(\frac{\Gamma_\rho}{m_\rho}\right)^2\rho_B - \frac{1}{2}\left(\frac{\Gamma_\delta}{m_\delta}\right)^2\\ &\quad\times\frac{M^{*2}\rho_B}{\tilde{E}_F^2[1 + \left(\frac{\Gamma_\delta}{m_\delta}\right)^2 A(k_F, M^*)]},\end{aligned}\tag{68}$$

with notations similarly defined as in the nonlinear RMF model.

C. The nonlinear point-coupling RMF model

1. Lagrangian density

The point-coupling model is defined by a Lagrangian density that consists of only nucleon fields. In the present study, we use the Lagrangian density of the nonlinear point-coupling model of Refs.[48, 49], i.e.,

$$\mathcal{L}_{\rm NLPC} = \mathcal{L}^{\rm free} + \mathcal{L}^{\rm 4f} + \mathcal{L}^{\rm hot} + \mathcal{L}^{\rm der}, \tag{69}$$

with

$$\mathcal{L}^{\rm free} = \bar{\psi}(\mathrm{i}\gamma_\mu\partial^\mu - M)\psi, \quad (70)$$

$$\mathcal{L}^{\rm 4f} = -\frac{1}{2}\alpha_{\rm S}(\bar{\psi}\psi)(\bar{\psi}\psi) - \frac{1}{2}\alpha_{\rm V}(\bar{\psi}\gamma_\mu\psi)(\bar{\psi}\gamma^\mu\psi) - \frac{1}{2}\alpha_{\rm TS}(\bar{\psi}\vec{\tau}\psi)\cdot(\bar{\psi}\vec{\tau}\psi) - \frac{1}{2}\alpha_{\rm TV}(\bar{\psi}\vec{\tau}\gamma_\mu\psi)\cdot(\bar{\psi}\vec{\tau}\gamma^\mu\psi), \quad (71)$$

$$\mathcal{L}^{\rm hot} = -\frac{1}{3}\beta_{\rm S}(\bar{\psi}\psi)^3 - \frac{1}{4}\gamma_{\rm S}(\bar{\psi}\psi)^4 - \frac{1}{4}\gamma_{\rm V}[(\bar{\psi}\gamma_\mu\psi)(\bar{\psi}\gamma^\mu\psi)]^2 - \frac{1}{4}\gamma_{\rm TV}[(\bar{\psi}\vec{\tau}\gamma_\mu\psi)\cdot(\bar{\psi}\vec{\tau}\gamma^\mu\psi)]^2, \quad (72)$$

$$\mathcal{L}^{\rm der} = -\frac{1}{2}\delta_{\rm S}(\partial_\nu\bar{\psi}\psi)(\partial^\nu\bar{\psi}\psi) - \frac{1}{2}\delta_{\rm V}(\partial_\nu\bar{\psi}\gamma_\mu\psi)(\partial^\nu\bar{\psi}\gamma^\mu\psi) - \frac{1}{2}\delta_{\rm TS}(\partial_\nu\bar{\psi}\vec{\tau}\psi)\cdot(\partial^\nu\bar{\psi}\vec{\tau}\psi) - \frac{1}{2}\delta_{\rm TV}(\partial_\nu\bar{\psi}\vec{\tau}\gamma_\mu\psi)\cdot(\partial^\nu\bar{\psi}\vec{\tau}\gamma^\mu\psi). \quad (73)$$

In the above, $\mathcal{L}^{\rm free}$ is the kinetic term of nucleons and $\mathcal{L}^{\rm 4f}$ describes the four-fermion interactions while $\mathcal{L}^{\rm hot}$ and $\mathcal{L}^{\rm der}$ contain, respectively, higher-order terms involving more than four fermions and derivatives in the nucleon field. For the twelve coupling constants in the Lagrangian density, $\alpha_{\rm S}$, $\alpha_{\rm V}$, $\alpha_{\rm TS}$, $\alpha_{\rm TV}$, $\beta_{\rm S}$, $\gamma_{\rm S}$, $\gamma_{\rm V}$, $\gamma_{\rm TV}$, $\delta_{\rm S}$, $\delta_{\rm V}$, $\delta_{\rm TS}$, and $\delta_{\rm TV}$, the subscripts denote the tensor structure of a coupling with "S" "V" and "T" stand for scalar, vector, and isovector, respectively. The symbols $\alpha_{\rm i}$, $\delta_{\rm i}$, $\beta_{\rm i}$, and $\gamma_{\rm i}$ refer, respectively, to four-fermion or second-order terms, derivative couplings, third- and fourth order terms [48, 49].

2. Equation of motion and nucleon self-energies

From the variation of the Lagrangian density Eq. (69) with respect to $\bar{\psi}$, we obtain the following Dirac equation for the nucleon field:

$$[\gamma_\mu(i\partial^\mu - \Sigma^\mu) - (M + \Sigma^S)]\psi = 0, \quad (74)$$

where the nucleon scalar (Σ^S) and vector (Σ^μ) self-energies are

$$\Sigma^S = V_S + \vec{V}_{TS}\cdot\vec{\tau}, \quad (75)$$

$$\Sigma^\mu = V^\mu + \vec{V}^\mu_T\cdot\vec{\tau}, \quad (76)$$

respectively, with

$$V_S = \alpha_{\rm S}(\bar{\psi}\psi) + \beta_{\rm S}(\bar{\psi}\psi)^2 + \gamma_{\rm S}(\bar{\psi}\psi)^3 - \delta_{\rm S}\Box(\bar{\psi}\psi), \quad (77)$$

$$\vec{V}_{TS} = \alpha_{\rm TS}(\bar{\psi}\vec{\tau}\psi) - \delta_{\rm TS}\Box(\bar{\psi}\vec{\tau}\psi), \quad (78)$$

$$V^\mu = \alpha_{\rm V}(\bar{\psi}\gamma^\mu\psi) + \gamma_{\rm V}(\bar{\psi}\gamma^\mu\psi)(\bar{\psi}\gamma_\mu\psi)(\bar{\psi}\gamma^\mu\psi) - \delta_{\rm V}\Box(\bar{\psi}\gamma^\mu\psi), \quad (79)$$

$$\vec{V}^\mu_T = \alpha_{\rm TV}(\bar{\psi}\vec{\tau}\gamma^\mu\psi) + \gamma_{\rm TV}(\bar{\psi}\vec{\tau}\gamma^\mu\psi)\cdot(\bar{\psi}\vec{\tau}\gamma_\mu\psi)(\bar{\psi}\vec{\tau}\gamma^\mu\psi) - \delta_{\rm TV}\Box(\bar{\psi}\vec{\tau}\gamma^\mu\psi). \quad (80)$$

In the above, $\Box = \partial^2/(c^2\partial t^2 - \triangle)$ denotes the four-dimensional d'Alembertian. In the translationally invariant infinite nuclear matter, all terms involving derivative couplings drop out and the spatial components of the four-currents also vanish. In terms of the baryon density ρ_B and scalar density ρ_S as well as the isospin baryon density $\rho_3 = \rho_p - \rho_n$ and the isospin scalar density $\rho_{S3} = \rho_{S,p} - \rho_{S,n}$, the nucleon scalar and vector self-energies in asymmetric nuclear matter can be rewritten as

$$\Sigma^S_\tau = \alpha_{\rm S}\rho_S + \beta_{\rm S}\rho_S^2 + \gamma_{\rm S}\rho_S^3 + \alpha_{\rm TS}\rho_{S3}\tau_3, \quad (81)$$

$$\Sigma^0_\tau = \alpha_{\rm V}\rho_B + \gamma_{\rm V}\rho_B^3 + \alpha_{\rm TV}\rho_3\tau_3 + \gamma_{\rm TV}\rho_3^3\tau_3. \quad (82)$$

3. Nuclear matter equation of state

The energy density ϵ and the pressure P derived from the energy-momentum tensor in the nonlinear point-coupling RMF model are given by

$$\epsilon = \epsilon^n_{kin} + \epsilon^p_{kin} - \frac{1}{2}\alpha_{\rm S}\rho_S^2 - \frac{1}{2}\alpha_{\rm TS}\rho_{S3}^2 + \frac{1}{2}\alpha_{\rm V}\rho^2 + \frac{1}{2}\alpha_{\rm TV}\rho_3^2 - \frac{1}{3}\beta_{\rm S}\rho_S^3 - \frac{3}{4}\gamma_{\rm S}\rho_S^4 + \frac{1}{4}\gamma_{\rm V}\rho^4 + \frac{1}{4}\gamma_{\rm TV}\rho_3^4, \quad (83)$$

$$P = \tilde{E}^p_F\rho_p + \tilde{E}^n_F\rho_n - \epsilon^p_{kin} - \epsilon^n_{kin} + \frac{1}{2}\alpha_{\rm S}\rho_s^2 + \frac{1}{2}\alpha_{\ \rm TS}\rho_{s3}^2 + \frac{1}{2}\alpha_{\rm V}\rho^2 + \frac{1}{2}\alpha_{\rm TV}\rho_3^2 + \frac{2}{3}\beta_{\rm S}\rho_s^3 + \frac{3}{4}\gamma_{\rm S}\rho_s^4 + \frac{3}{4}\gamma_{\rm V}\rho^4 + \frac{3}{4}\gamma_{\rm TV}\rho_3^4, \quad (84)$$

where $\tilde{E}^p_F$ and $\tilde{E}^n_F$ are defined as in Eq. (36) with the nucleon Dirac masses

$$M^*_p = \alpha_{\rm S}\rho_S + \beta_{\rm S}\rho_S^2 + \gamma_{\rm S}\rho_S^3 + \alpha_{\rm TS}\rho_{S3}, \quad (85)$$

$$M^*_n = \alpha_{\rm S}\rho_S + \beta_{\rm S}\rho_S^2 + \gamma_{\rm S}\rho_S^3 - \alpha_{\rm TS}\rho_{S3}. \quad (86)$$

Furthermore, the symmetry energy in this model can be expressed as

$$E_{\rm sym}(\rho_B) = \frac{k_F^2}{6\tilde{E}_F} + \frac{1}{2}\alpha_{\rm TV}\rho_B + \frac{1}{2}\alpha_{\rm TS}\frac{M^{*2}\rho_B}{\tilde{E}_F^2[1 - \alpha_{\rm TS}A(k_F, M^*)]}, \quad (87)$$

with notations again similarly defined as in the nonlinear RMF model.

D. The density-dependent point-coupling RMF model

1. Lagrangian density

For the density-dependent point-coupling RMF model, we use the Lagrangian density of Refs.[52, 53], i.e.,

$$\mathcal{L}_{\rm DDPC} = \mathcal{L}_{\rm free} + \mathcal{L}_{\rm 4f} + \mathcal{L}_{\rm der}, \tag{88}$$

with

$$\begin{aligned}
\mathcal{L}_{\rm free} &= \bar{\psi}(i\gamma_\mu\partial^\mu - M)\psi, && (89)\\
\mathcal{L}_{\rm 4f} &= -\frac{1}{2}\,G_S(\hat{\rho})(\bar{\psi}\psi)(\bar{\psi}\psi) \\
&\quad -\frac{1}{2}\,G_V(\hat{\rho})(\bar{\psi}\gamma_\mu\psi)(\bar{\psi}\gamma^\mu\psi) \\
&\quad -\frac{1}{2}\,G_{TS}(\hat{\rho})(\bar{\psi}\vec{\tau}\psi)\cdot(\bar{\psi}\vec{\tau}\psi) \\
&\quad -\frac{1}{2}\,G_{TV}(\hat{\rho})(\bar{\psi}\vec{\tau}\gamma_\mu\psi)\cdot(\bar{\psi}\vec{\tau}\gamma^\mu\psi), && (90)\\
\mathcal{L}_{\rm der} &= -\frac{1}{2}\,D_S(\hat{\rho})(\partial_\nu\bar{\psi}\psi)(\partial^\nu\bar{\psi}\psi). && (91)
\end{aligned}$$

In the above, $\mathcal{L}^{\rm free}$ is the kinetic term of the nucleons and $\mathcal{L}^{\rm 4f}$ is a four-fermion interaction while $\mathcal{L}^{\rm der}$ represents derivatives in the nucleon scalar densities. Unlike in the nonlinear point-coupling RMF model, the density-dependent point-coupling RMF model used here includes only second-order interaction terms with density-dependent couplings $G_i(\hat{\rho})$ and $D_i(\hat{\rho})$ that are determined from finite-density QCD sum rules and in-medium chiral perturbation theory [52, 53].

2. Equation of motion and nucleon self-energies

Variation of the Lagrangian Eq.(88) with respect to $\bar{\psi}$ leads to the single-nucleon Dirac equation

$$[\gamma_\mu(i\partial^\mu - \Sigma^\mu) - (M + \Sigma^S)]\psi = 0, \tag{92}$$

with the nucleon scalar and vector self-energies given, respectively, by

$$\begin{aligned}
\Sigma^S &= V_S + \vec{V}_{TS}\cdot\vec{\tau} + \Sigma_{rS}\ , && (93)\\
\Sigma^\mu &= V^\mu + \vec{V}^\mu_T\cdot\vec{\tau} + \Sigma^\mu_r, && (94)
\end{aligned}$$

where

$$\begin{aligned}
V_S &= G_S(\bar{\psi}\psi) - D_S\Box(\bar{\psi}\psi), && (95)\\
\vec{V}_{TS} &= G_{TS}(\bar{\psi}\vec{\tau}\psi), && (96)\\
V^\mu &= G_V(\bar{\psi}\gamma^\mu\psi), && (97)\\
\vec{V}^\mu_T &= G_{TV}(\bar{\psi}\vec{\tau}\gamma^\mu\psi), && (98)\\
\Sigma_{rS} &= -\frac{\partial D_S}{\partial\hat{\rho}}(\partial_\nu j^\mu)u_\mu(\partial^\nu(\bar{\psi}\psi)) && (99)
\end{aligned}$$

and

$$\begin{aligned}
\Sigma^\mu_r &= \frac{u^\mu}{2}\left(\frac{\partial G_S}{\partial\hat{\rho}}(\bar{\psi}\psi)(\bar{\psi}\psi) + \frac{\partial G_{TS}}{\partial\hat{\rho}}(\bar{\psi}\vec{\tau}\psi)\cdot(\bar{\psi}\vec{\tau}\psi)\right. \\
&\quad + \frac{\partial G_V}{\partial\hat{\rho}}(\bar{\psi}\gamma^\mu\psi)(\bar{\psi}\gamma_\mu\psi) + \frac{\partial G_{TV}}{\partial\hat{\rho}}(\bar{\psi}\vec{\tau}\gamma^\mu\psi)\cdot(\bar{\psi}\vec{\tau}\gamma_\mu\psi) \\
&\quad \left. + \frac{\partial D_S}{\partial\hat{\rho}}(\partial^\nu(\bar{\psi}\psi))(\partial_\nu(\bar{\psi}\psi))\right). && (100)
\end{aligned}$$

In the above, we have $\hat{\rho}u^\mu = \bar{\psi}\gamma^\mu\psi$, where the four-velocity u^μ is defined as $(1-\mathbf{v}^2)^{-1/2}(1,\mathbf{v})$ with $\mathbf{v}$ being the three-velocity vector, and Σ_{rS} and Σ^μ_r represent the rearrangement contributions resulting from the variation of the vertex functionals with respect to the nucleon fields in the density operator $\hat{\rho}$. The latter coincides with the baryon density in the nuclear matter rest frame.

In the translationally invariant infinite asymmetric nuclear matter, the nucleon scalar and vector self-energies become

$$\begin{aligned}
\Sigma^S_\tau &= G_S\rho_S + G_{TS}\rho_{S3}\tau_3 && (101)\\
\Sigma^0_\tau &= G_V\rho_B + G_{TV}\rho_3\tau_3 + \Sigma^{0(R)}, && (102)
\end{aligned}$$

with the rearrangement contribution to the self-energy

$$\Sigma^{0(R)} = \frac{1}{2}[\frac{\partial G_S}{\partial\rho}\rho_S^2 + \frac{\partial G_{TS}}{\partial\rho}\rho_{S3}^2 + \frac{\partial G_V}{\partial\rho}\rho^2 + \frac{\partial G_{TV}}{\partial\rho}\rho_3^2]. \tag{103}$$

3. Nuclear matter equation of state

For asymmetric nuclear matter, the energy density ϵ and the pressure P derived from the energy-momentum tensor in the density-dependent point-coupling RMF model are

$$\begin{aligned}
\epsilon &= \epsilon^n_{kin} + \epsilon^p_{kin} - \frac{1}{2}G_S\rho_S^2 - \frac{1}{2}G_{TS}\rho_{S3}^2 \\
&\quad + \frac{1}{2}G_V\rho^2 + \frac{1}{2}G_{TV}\rho_3^2, && (104)
\end{aligned}$$

and

$$\begin{aligned}
P &= \tilde{E}^p_F\rho_p + \tilde{E}^n_F\rho_n - \epsilon^p_{kin} - \epsilon^n_{kin} \\
&\quad + \frac{1}{2}G_V\rho^2 + \frac{1}{2}G_{TV}\rho_3^2 + \frac{1}{2}G_S\rho_S^2 + \frac{1}{2}G_{TS}\rho_{S3}^2 \\
&\quad + \frac{1}{2}\frac{\partial G_S}{\partial\rho}\rho_S^2\rho + \frac{1}{2}\frac{\partial G_V}{\partial\rho}\rho^3 \\
&\quad + \frac{1}{2}\frac{\partial G_{TV}}{\partial\rho}\rho_3^2\rho + \frac{1}{2}\frac{\partial G_{TS}}{\partial\rho}\rho_{S3}^2\rho, && (105)
\end{aligned}$$

where $\tilde{E}^p_F$ and $\tilde{E}^n_F$ are defined as in Eq. (36) with the effective nucleon masses

$$\begin{aligned}
M^*_p &= M + G_S\rho_S + G_{TS}\rho_{S3}, && (106)\\
M^*_n &= M + G_S\rho_S - G_{TS}\rho_{S3}. && (107)
\end{aligned}$$

As in the density-dependent RMF model, *rearrangement* contributions appear explicitly in the expression for the

pressure. Finally, the symmetry energy can be written as

$$E_{\rm sym}(\rho_B) = \frac{k_F^2}{6\tilde{E}_F} + \frac{1}{2}G_{TV}\rho_B + \frac{1}{2}G_{TS}\frac{M^{*2}\rho_B}{\tilde{E}_F^2[1-G_{TS}A(k_F,M^*)]}, \quad (108)$$

with similar notations as in the nonlinear RMF model.

IV. RESULTS AND DISCUSSIONS

Using above models, we have studied the isospin-dependent properties of asymmetric nuclear matter. In the following, we focus on results regarding the nuclear symmetry energy, the nuclear symmetry potential, the isospin-splitting of nucleon effective mass, and the isospin-dependent nucleon scalar density in asymmetric nuclear matter. For different versions of the RMF model considered in the present work, we mainly consider parameter sets commonly and successfully used in nuclear structure studies. In particular, we select the parameter sets NL1 [102], NL2 [102], NL3 [103], NL-SH [104], TM1 [105], PK1 [106], FSU-Gold [76], HA [107], NLρ [100], NL$\rho\delta$ [100] for the nonlinear RMF model; TW99 [46], DD-ME1 [108], DD-ME2 [109], PKDD [106], DD [93], DD-F [110], and DDRH-corr [47] for the density-dependent RMF model; and PC-F1 [49], PC-F2 [49], PC-F3 [49], PC-F4 [49], PC-LA [49], and FKVW [53] for the point-coupling RMF model. There are totally 23 parameter sets, and most of them can describe reasonably well the binding energies and charge radii of a large number of nuclei in the periodic table except the parameter set HA, for which to our knowledge there are no calculations for finite nuclei.

We note that all selected parameter sets include the isovector-vector channel involving either the isovector-vector ρ meson or the isovector-vector interaction vertices in the Lagrangian. The HA parameter set further includes the isovector-scalar meson field $\vec{\delta}$ and fits successfully some results obtained from the more microscopic DBHF approach [107]. The parameter sets NL$\rho\delta$ and DDRH-corr also include the isovector-scalar meson field $\vec{\delta}$, while PC-F2, PC-F4, PC-LA, and FKVW include the isovector-scalar interaction vertices. The parameter sets NL$\rho\delta$ as well as NLρ are obtained from fitting the empirical properties of asymmetric nuclear matter [100] and describe reasonably well the binding energies and charge radii of a large number of nuclei [111]. For the DDRH-corr, its parameters are determined from the density-dependent meson-nucleon vertices extracted from the self-energies of asymmetric nuclear matter calculated in the microscopic DBHF approach with momentum corrections, and it reproduces satisfactorily the properties of finite nuclei and the EOS from the DBHF approach [47]. In the parameter sets PC-F1, PC-F2, PC-F3, PC-F4 and PC-LA for the nonlinear point-coupling model, their coupling constants are determined in a self-consistent procedure that solves the model equations for representative nuclei simultaneously in a generalized nonlinear least-squares adjustment algorithm [49]. The parameter set FKVW for the density-dependent point-coupling model are determined by the constraints derived from the finite-density QCD sum rules, in-medium chiral perturbation theory, and experimental data of a number of finite nuclei [53].

A. Nuclear symmetry energy

Fig. 1 displays the density dependence of the nuclear symmetry energy $E_{\rm sym}(\rho)$ for the 23 parameter sets in the nonlinear, density-dependent, and point-coupling RMF models. For comparison, we also show in Fig. 1 results from the phenomenological parametrization of the momentum-dependent nuclear mean-field potential based on the Gogny effective interaction [25], i.e., the MDI interactions with $x = -1$ (open squares) and 0 (solid squares), where different x values correspond to different density dependence of the nuclear symmetry energy but keep other properties of the nuclear EOS the same [55] (see Appendix A for details). From analyzing the isospin diffusion data from NSCL/MSU using the IBUU04 transport model with in-medium NN cross sections, it has been found that the MDI interactions with $x = -1$ and 0 give, respectively, the upper and lower bounds for the stiffness of the nuclear symmetry energy at densities up to about $1.2\rho_0$ [55, 56].

It is seen from Fig. 1 that the density dependence of symmetry energy varies drastically among different interactions. In the nonlinear RMF model, while the dependence on density is almost linear for most parameter sets, it is much softer for the parameter sets FSU-Gold and HA. The softening of the symmetry energy from the latter two parameter sets is due to the mixed isoscalar-isovector couplings Λ_S and Λ_V [66, 99] which modifies the density dependence of symmetry energy as seen in Eq. (44). For the parameter set NL$\rho\delta$, it gives a symmetry energy that depends linearly on density at low densities but becomes stiffer at high densities due to inclusion of the isovector-scalar δ meson. The approximate linear density-dependent behavior of the symmetry energy for other parameter sets in the nonlinear RMF model can also be understood from Eq. (44), which shows that the symmetry energy at high densities is dominated by the potential energy that is proportional to the baryon density if the mixed isoscalar-isovector coupling and the isovector-scalar δ meson are not included in the model.

The density dependence of the symmetry energy in the density-dependent RMF model is essentially determined by the density dependence of the coupling constants Γ_ρ and Γ_δ of isovector mesons. Most parameter sets in this case give similar symmetry energies except the parameter sets PKDD and DDRH-corr. Compared with other parameter sets in the density-dependent RMF

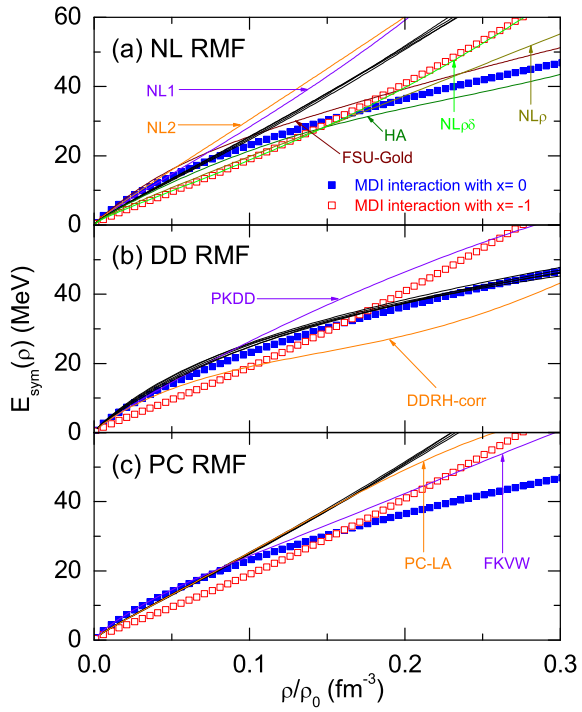

FIG. 1: (Color online) Density dependence of the nuclear symmetry energy $E_{\rm sym}(\rho)$ for the parameter sets NL1, NL2, NL3, NL-SH, TM1, PK1, FSU-Gold, HA, NLρ, and NL$\rho\delta$ in the nonlinear RMF model (a); TW99, DD-ME1, DD-ME2, PKDD, DD, DD-F, and DDRH-corr in the density-dependent RMF model (b); and PC-F1, PC-F2, PC-F3, PC-F4, PC-LA, and FKVW in the point-coupling RMF model (c). For comparison, results from the MDI interaction with $x = -1$ (open squares) and 0 (solid squares) are also shown.

model, PKDD gives a very large while DDRH-corr gives a very small value for the symmetry energy at saturation density. For point-coupling models, all parameter sets (PC-F1, PC-F2, PC-F3, PC-F4 and PC-LA) in the nonlinear point-coupling RMF model predict almost linearly density-dependent symmetry energies while the parameter set FKVW in the density-dependent point-coupling RMF model gives a somewhat softer symmetry energy.

Fig. 1 thus shows that only a few parameter sets can give symmetry energies that are consistent with the constraint from the isospin diffusion data in heavy-ion collisions, which is given by results from the MDI interactions with $x = -1$ and 0. The main reason for this is that most parameter sets in the RMF model have saturation densities and symmetry energies at their saturation densities which are significantly different from the empirical saturation density of 0.16 fm^{-3} and symmetry energy of 31.6 MeV at this saturation density. To show this more clearly, we list in Table I the bulk properties of nuclear matter at saturation density: the binding energy per nucleon $-B/A$ (MeV), the saturation density of symmetric nuclear matter ρ_0 (fm^{-3}), the incompressibility of symmetric nuclear matter K_0 (MeV), the symmetry energy $E_{\rm sym}(\rho_0)$ (MeV), $K_{\rm sym}$ (MeV), L (MeV), and $K_{\rm asy}$ (MeV) using the 23 parameter sets in the nonlinear, density-dependent, and point-coupling RMF models. It is seen that these parameter sets give saturation densities varying from $\rho_0 = 0.145$ fm^{-3} to $\rho_0 = 0.180$ fm^{-3} and nuclear symmetry energies $E_{\rm sym}(\rho_0)$ (MeV) ranging from 26.1 to 44.0 MeV.

TABLE I: Bulk properties of nuclear matter at the saturation point: $-B/A$ (MeV), ρ_0 (fm^{-3}), K_0 (MeV), $E_{\rm sym}$ (ρ_0) (MeV), $K_{\rm sym}$ (MeV), L (MeV), and $K_{\rm asy}$ (MeV) using the 23 parameter sets in the nonlinear, density-dependent, and point-coupling RMF models. The last column gives the references for corresponding parameter sets.

Model	$-B/A$	ρ_0	K_0	$E_{\rm sym}$	L	$K_{\rm sym}$	$K_{\rm asy}$	Ref.
NL1	16.4	0.152	212	43.5	140	143	−697	[102]
NL2	17.0	0.146	401	44.0	130	20	−750	[102]
NL3	16.2	0.148	271	37.3	118	100	−608	[103]
NL-SH	16.3	0.146	356	36.1	114	80	−604	[104]
TM1	16.3	0.145	281	36.8	111	34	−632	[105]
PK1	16.3	0.148	282	37.6	116	55	−641	[106]
FSUGold	16.3	0.148	229	32.5	60	−52	−412	[76]
HA	15.6	0.170	233	30.7	55	−135	−465	[107]
NLρ	16.1	0.160	240	30.3	85	3	−507	[100]
NL$\rho\delta$	16.1	0.160	240	30.7	103	127	−491	[100]
TW99	16.2	0.153	241	32.8	55	−124	−454	[46]
DD-ME1	16.2	0.152	245	33.1	55	−101	−431	[108]
DD-ME2	16.1	0.152	251	32.3	51	−87	−393	[109]
PKDD	16.3	0.150	263	36.9	90	−80	−620	[106]
DD	16.0	0.149	241	31.7	56	−95	−431	[93]
DD-F	16.0	0.147	223	31.6	56	−140	−476	[110]
DDRH-corr	15.6	0.180	281	26.1	51	155	−151	[47]
PC-F1	16.2	0.151	255	37.8	117	75	−627	[49]
PC-F2	16.2	0.151	256	37.6	116	65	−631	[49]
PC-F3	16.2	0.151	256	38.3	119	74	−640	[49]
PC-F4	16.2	0.151	255	37.7	119	98	−616	[49]
PC-LA	16.1	0.148	263	37.2	108	−61	−709	[49]
FKVW	16.2	0.149	379	33.1	80	11	−469	[53]

To remove the effect due to differences in the saturation densities among different parameter sets, we show in Fig. 2 both the symmetry energy $E_{\rm sym}(\rho)$ and the symmetry energy scaled by its value at corresponding saturation density, i.e., $E_{\rm sym}(\rho)/E_{\rm sym}(\rho_0)$ as functions of the scaled baryon density ρ/ρ_0 for different parameter sets. For comparison, we also plot in the inset in panel (b) of Fig. 2 the symmetry energy $E_{\rm sym}(\rho)$ as a function of the baryon density ρ without scaling. It is seen that more parameter sets among the 23 sets become consistent with the constraint from the isospin diffusion data in heavy-ion collisions after scaling the baryon density by the saturation density, and with further scaling of the

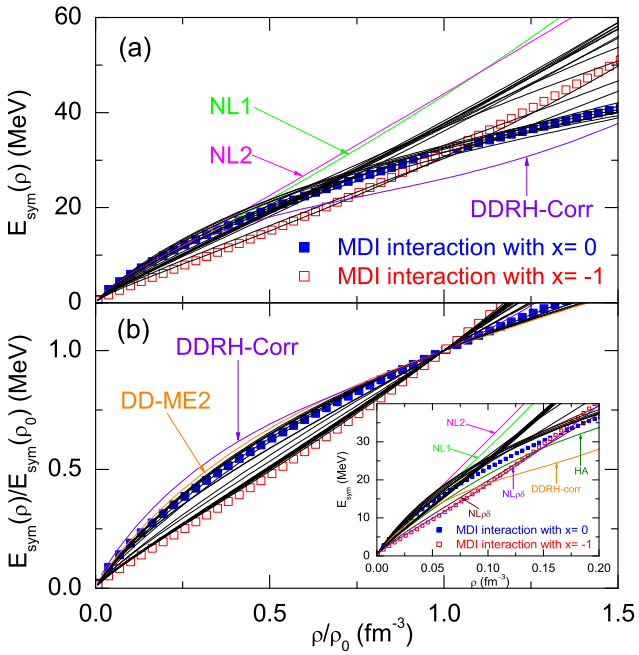

FIG. 2: (Color online) The symmetry energy $E_{\rm sym}(\rho)$ (a) and the scaled symmetry energy $E_{\rm sym}(\rho)/E_{\rm sym}(\rho_0)$ (b) as functions of the scaled baryon density ρ/ρ_0 for the 23 parameter sets in the nonlinear, density-dependent, and point-coupling RMF models. Results of the MDI interaction with $x = -1$ (open squares) and 0 (solid squares) are also included for comparison. The inset in panel (b) shows the symmetry energy $E_{\rm sym}(\rho)$ as a function of the baryon density ρ without scaling.

symmetry energy by its value at corresponding saturation density, most of the parameter sets are in agreement with the constraint from the isospin diffusion data. It is also interesting to see from the inset in Fig. 2 that most of the parameter sets obtained from fitting the properties of finite nuclei give roughly the same value of about 26 MeV for the nuclear symmetry energy at the same baryon density of $\rho = 0.1$ fm^{-3}. This interesting feature is very similar to that found with Skyrme interactions [64, 70]. It implies that the constraint on the symmetry energy from fitting the properties of finite nuclei is particularly sensitive to the nuclear properties at lower densities, i.e., at density slightly above half-saturation density.

For the density dependence of the nuclear symmetry energy around saturation density, a more reasonable and physically meaningful comparison is through the values of L and $K_{\rm asy}$ given by these parameter sets since the L parameter is correlated linearly to the neutron-skin thickness of finite nuclei while the $K_{\rm asy}$ parameter determines the isotopic dependence of the GMR for a fixed element. From Table I, we have seen that the values of L, $K_{\rm sym}$, and $K_{\rm asy}$ vary drastically, and they are in the range of $51 \sim 140$ MeV, $-140 \sim 143$ MeV and $-750 \sim -151$ MeV, respectively. The extracted values of $L = 88 \pm 25$ MeV and $K_{\rm asy} = -500 \pm 50$ MeV from the isospin diffusion data, $L \approx 65$ MeV and $K_{\rm asy} \approx -453$ MeV from the isoscaling data, and $K_{\rm asy} = -550 \pm 100$ MeV from the isotopic dependence of the GMR in even-A Sn isotopes give a rather stringent constraint on the density dependence of the nuclear symmetry energy and thus put strong constraints on the nuclear effective interactions as well. To see this constraint more clearly, we collect in Fig. 3 the values of L and $K_{\rm asy}$ obtained from the 23 parameter sets in the nonlinear, density-dependent, and point-coupling RMF models together with the constraints from the isospin diffusion data, isoscaling data, and the isotopic dependence of the GMR in even-A Sn isotopes. From Fig. 3 as well as Table I, we see clearly that among the 23 parameter sets considered here, only six sets, i.e., TM1, NLρ, NL$\rho\delta$, PKDD, PC-LA, and FKVW, have nuclear symmetry energies that are consistent with the extracted L value of 88±25 MeV while fifteen sets, i.e., NL3, NL-SH, TM1, PK1, HA, NLρ, NL$\rho\delta$, TW99, PKDD, DD-F, PC-F1, PC-F2, PC-F3, PC-F4, and FKVW, have nuclear symmetry energies that are consistent with the extracted $K_{\rm asy}$ value of -500 ± 50 MeV or -550 ± 100 MeV. Among the latter fifteen sets, only six sets, i.e., HA, NLρ, NL$\rho\delta$, TW99, DD-F, and FKVW are consistent with $K_{\rm asy} = -500 \pm 50$ MeV. It is interesting to see that most parameter sets in the nonlinear and point-coupling RMF models predict stiffer symmetry energies (i.e., larger values for the L parameter and larger magnitudes for $K_{\rm asy}$) while those in the density-dependent RMF model give softer symmetry energies (i.e., smaller values for the L parameter and smaller magnitudes for $K_{\rm asy}$).

We also see from Table I that only five parameter sets, i.e., TM1, NLρ, NL$\rho\delta$, PKDD and FKVW, in the 23 parameter sets have nuclear symmetry energies that are consistent with the extracted values for both L and $K_{\rm asy}$ (-500 ± 50 MeV or -550 ± 100 MeV). This can be seen more clearly in Fig. 4 where the correlation between L and $K_{\rm asy}$ is displayed for the 23 parameter sets together with the constraints from the isospin diffusion data, the isoscaling data, and the isotopic dependence of the GMR in even-A Sn isotopes. Fig. 4 further shows that there exists an approximately linear correlation between L and $K_{\rm asy}$, i.e., a larger L leads to a larger magnitude for $K_{\rm asy}$. A similar approximately linear correlation between L and $K_{\rm asy}$ has also been observed in Ref. [55] for the phenomenological MDI interactions, and this correlation can be understood from Eq. (7) which shows that the value of $K_{\rm asy}$ is more sensitive to the value of L than to that of $K_{\rm sym}$.

The above comparisons thus indicate that the extracted values of $L = 88 \pm 25$ MeV and $K_{\rm asy} = -500 \pm 50$ MeV from the isospin diffusion data, $L \approx 65$ MeV and $K_{\rm asy} \approx -453$ MeV from the isoscaling data, and $K_{\rm asy} = -550 \pm 100$ MeV from the isotopic dependence of the GMR in even-A Sn isotopes indeed put a very stringent constraint on the values of the parameters in different RMF models. The fact that most of the 23 parameter sets considered in the present work give sym-

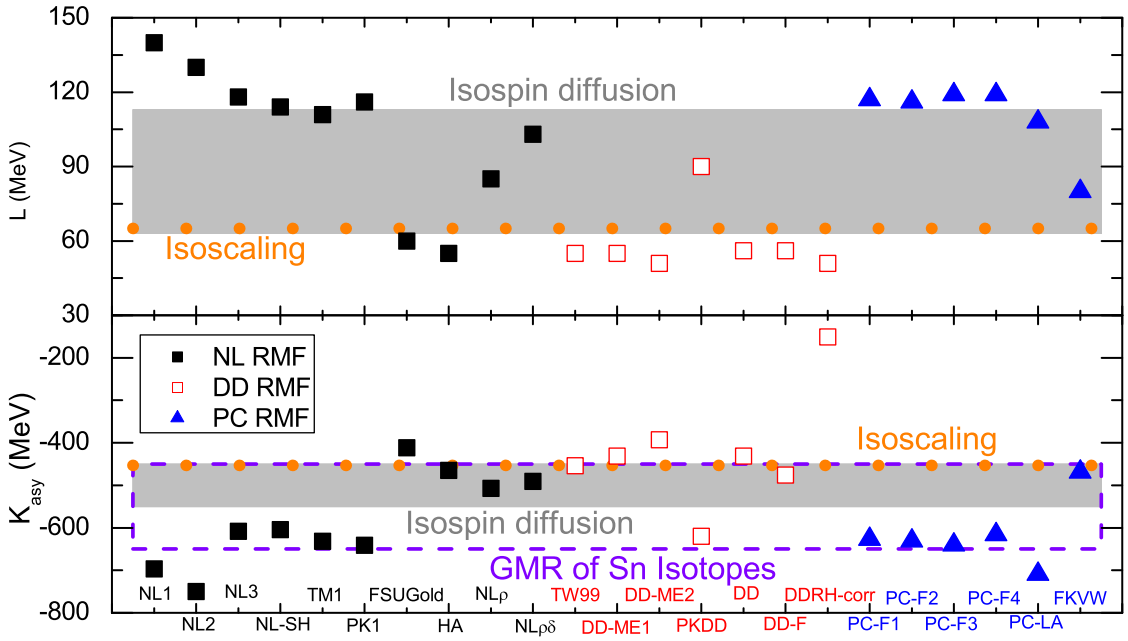

FIG. 3: (Color online) Values of L and $K_{\rm asy}$ for the 23 parameter sets in the nonlinear (solid squares), density-dependent (open squares), and point-coupling (triangles) RMF models. The constraints from the isospin diffusion data (shaded band), the isoscaling data (solid circles), and the isotopic dependence of the GMR in even-A Sn isotopes (dashed rectangle) are also included.

metry energies that are inconsistent with the constraints of $L = 88 \pm 25$ MeV and $K_{\rm asy} = -500 \pm 50$ MeV or -550 ± 100 MeV is probably related to the rather limited flexibility in the parametrization of the isovector channel in all RMF models. They are also probably connected to the fact that most of the parameter sets are obtained from fitting properties of finite nuclei, which are mostly near the β-stability line and thus are not well constrained by the isospin-dependent properties of nuclear EOS. Also, we are interested here in the density-dependent behavior of the symmetry energy around saturation density, as both L and $K_{\rm asy}$ are defined at saturation density, while the behavior of the nuclear EOS at sub-subsaturation density may be more relevant when the parameter sets are obtained from fitting the properties of finite nuclei.

B. Nuclear symmetry potential

Using the parameter sets NL1, NL2, NL3, NL-SH, TM1, PK1, FSU-Gold, HA, NLρ, and NL$\rho\delta$ in the nonlinear RMF model, we have evaluated the energy dependence of the three different nucleon optical potentials, i.e., the "Schrödinger-equivalent potential" $U_{\rm SEP}$ (Eq. (10)), the optical potential from the difference between the total energy of a nucleon in nuclear medium and its energy at the same momentum in free space $U_{\rm OPT}$ (Eq. (12)), and the optical potential based on the second-order Dirac equation $U_{\rm SOD}$ (Eq. (15)), at a fixed baryon density $\rho_B = 0.16$ fm^{-3} (roughly corresponding to the saturation densities obtained from various RMF models). For their corresponding symmetry potentials $U_{\rm sym}^{\rm SEP}$, $U_{\rm sym}^{\rm OPT}$, and $U_{\rm sym}^{\rm SOD}$, we have evaluated instead their dependence on the nucleon momentum in asymmetric nuclear matter at baryon density $\rho_B = 0.16$ fm^{-3} and with isospin asymmetry $\alpha = 0.5$. We note that in contrast to the energy dependence of the nuclear symmetry potential, the momentum dependence of the nuclear symmetry potential is almost independent of the isospin asymmetry of nuclear matter. These results are shown in Fig. 5. Corresponding results for the parameter sets TW99, DD-ME1, DD-ME2, PKDD, DD, DD-F, and DDRH-corr in the density-dependent RMF model and for PC-F1, PC-F2, PC-F3, PC-F4, PC-LA, and FKVW in the point-coupling RMF model are shown in Figs. 6 and 7, respectively. For comparison, we also include in these figures results for the energy dependence of the real part of the different optical potentials in symmetric nuclear matter at saturation density that are extracted from the proton-nucleus scattering data based on the Dirac phenomenology [82, 112].

It is seen that different optical potentials in symmetric nuclear matter at $\rho_B = 0.16$ fm^{-3} exhibit similar energy dependence at low energies but have different behaviors at high energies. In particular, at high energies, $U_{\rm SEP}$ continues to increase linearly with energy while $U_{\rm OPT}$ and $U_{\rm SOD}$ seem to saturate at high energies and thus display a more satisfactory high-energy limit, similar to

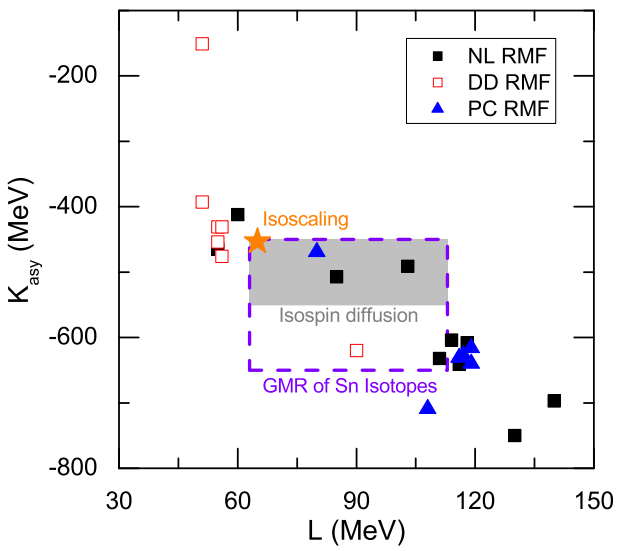

FIG. 4: (Color online) Correlation between L and $K_{\rm asy}$ for the 23 parameter sets in the nonlinear (solid squares), density-dependent (open squares), and point-coupling (triangles) RMF models. The constraints from the isospin diffusion data (shaded band), the isoscaling data (stars), and the isotopic dependence of the GMR in even-A Sn isotopes (dashed rectangle with L constrained by the isospin diffusion data) are also included.

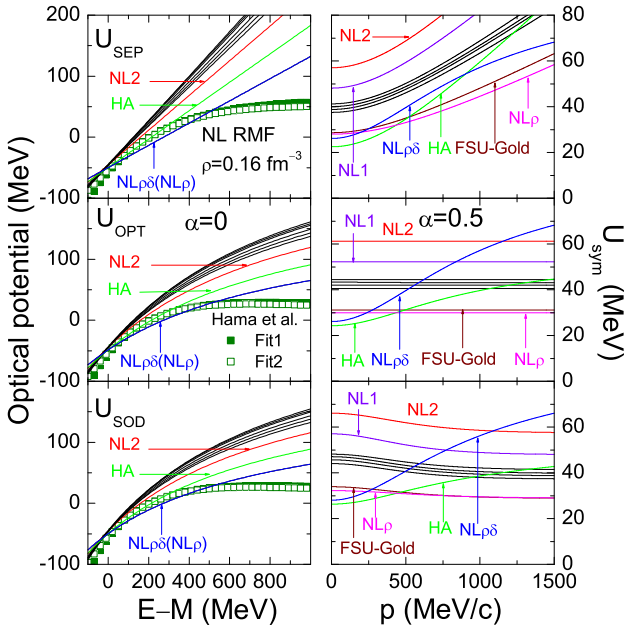

FIG. 5: (Color online) Energy dependence of the three different nucleon optical potentials, i.e., $U_{\rm SEP}$ (Eq. (10)), $U_{\rm OPT}$ (Eq. (12)) and $U_{\rm SOD}$ (Eq. (15)) (left panels) as well as their corresponding symmetry potentials $U_{\rm sym}^{\rm SEP}$, $U_{\rm sym}^{\rm OPT}$, and $U_{\rm sym}^{\rm SOD}$as functions of momentum (right panels), at a fixed baryon density $\rho_B = 0.16$ fm^{-3} for the parameter sets NL1, NL2, NL3, NL-SH, TM1, PK1, FSU-Gold, HA, NLρ, and NL$\rho\delta$ in the nonlinear RMF model. For comparison, the energy dependence of the real part of the optical potential in symmetric nuclear matter at saturation density extracted from two different fits of the proton-nucleus scattering data in the Dirac phenomenology are also included (left panels).

what is observed in the nuclear optical potential that is extracted from the experimental data based on the Dirac phenomenology. The critical energy at which the optical potential changes from negative to positive values is between about 130 MeV and 270 MeV, depending on the parameter sets used. These features are easy to understand from the fact that the scalar and vector potentials are momentum/energy-independent in the RMF models considered here. Analysis of experimental data from the proton-nucleus scattering in the Dirac phenomenology also indicates that the extracted different nucleon optical potentials in symmetric nuclear matter at normal nuclear density change from negative to positive values at a nucleon energy of about 208 MeV. Furthermore, it is seen that the different optical potentials from all 23 parameter sets are consistent with the experimental data at lower energies, i.e., $E_{\rm kin} < 100 - 200$ MeV, but are generally too repulsive at higher energies, especially for the "Schrödinger-equivalent potential" $U_{\rm SEP}$. These features imply that the RMF models with parameters fitted to the properties of finite nuclei can only give reasonable description of the low energy behavior of the isoscalar optical potentials. On the other hand, it should be mentioned that for optical potentials at high energies, contributions from dispersive processes such as dynamical polarization by inelastic excitations, inelastic isobar resonance excitation above the pion threshold, and particle production become important [113, 114]. Including such continuum excitations is expected to improve significantly the high energy behavior of the optical potential [113]. Such studies are, however, beyond the RMF model based on the Hartree level as considered here.

For the momentum dependence of the symmetry potential, all 23 parameter sets display similar behaviors in $U_{\rm sym}^{\rm SEP}$, i.e., increasing with momentum, albeit at different rates. This can be qualitatively understood as follows. Expressing Eq. (10) as

$$U_{{\rm SEP},\tau} = \frac{1}{2M_\tau}[E_\tau^2 - (M_\tau^2 + \vec{p}^2)], \qquad (109)$$

and neglecting the difference in neutron and proton

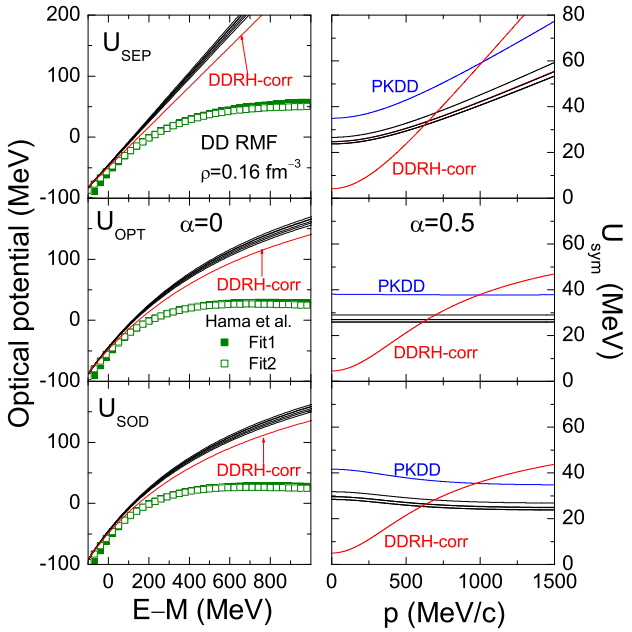

FIG. 6: (Color online) Same as Fig. 5 for TW99, DD-ME1, DD-ME2, PKDD, DD, DD-F, and DDRH-corr in the density-dependent RMF models.

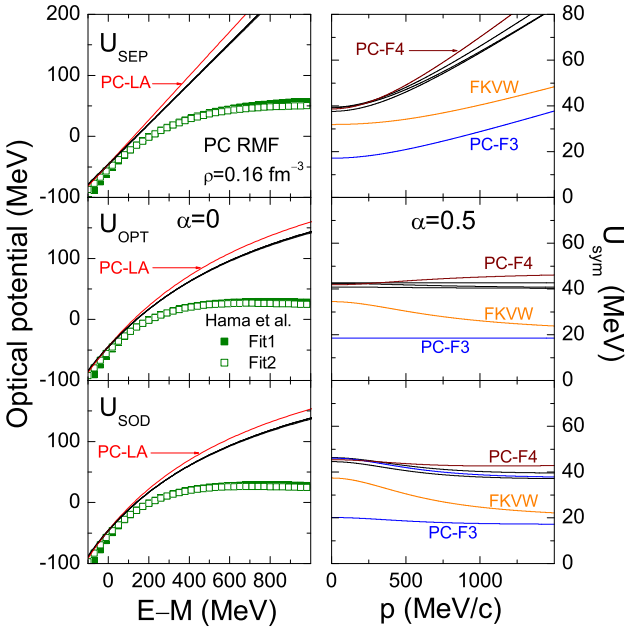

FIG. 7: (Color online) Same as Fig. 5 for PC-F1, PC-F2, PC-F3, PC-F4, PC-LA, and FKVW in the point-coupling RMF models.

masses, we can rewrite Eq. (11) as

$$\begin{aligned} U_{\rm sym}^{\rm SEP} &= \frac{E_n^2-E_p^2}{4M_\tau\alpha} \\ &= \frac{1}{4M_\tau\alpha}[(\Sigma_n^0)^2+2\Sigma_n^0\sqrt{\vec{p}^2+(M_n+\Sigma_n^S)^2} \\ &\quad +(M_n+\Sigma_n^S)^2-(\Sigma_p^0)^2 \\ &\quad -2\Sigma_p^0\sqrt{\vec{p}^2+(M_p+\Sigma_p^S)^2}-(M_p+\Sigma_p^S)^2] \\ &= \frac{1}{4M_\tau\alpha}[(\Sigma_n^0)^2-(\Sigma_p^0)^2+(M^*_{{\rm Dirac},n})^2 \\ &\quad -(M^*_{{\rm Dirac},p})^2+2\Sigma_n^0\sqrt{\vec{p}^2+(M^*_{{\rm Dirac},n})^2} \\ &\quad -2\Sigma_p^0\sqrt{\vec{p}^2+(M^*_{{\rm Dirac},p})^2}]. \end{aligned} \tag{110}$$

In the simple case of the nonlinear RMF model without the isovector-scalar δ meson, the neutron Dirac mass is the same as that of proton. In this case, $U_{\rm sym}^{\rm SEP}$ is reduced to

$$\begin{aligned} U_{\rm sym}^{\rm SEP} &= \frac{1}{4M_\tau\alpha}[(\Sigma_n^0)^2-(\Sigma_p^0)^2 \\ &\quad +2(\Sigma_n^0-\Sigma_p^0)\sqrt{\vec{p}^2+(M^*_{\rm Dirac})^2}]. \end{aligned} \tag{111}$$

Since it can be shown from Eqs. (31), (33), and (39) that

$$\Sigma_n^0-\Sigma_p^0=2\left(\frac{g_\rho}{m_\rho}\right)^2(\rho_n-\rho_p), \tag{112}$$

we thus have $\Sigma_n^0>\Sigma_p^0$ and an increase of $U_{\rm sym}^{\rm SEP}$ with the momentum of a nucleon in neutron-rich nuclear matter. The same argument applies to density-dependent RMF models and point-coupling models if the coupling constant $\alpha_{\rm TV}$ or G_{TV} in the point-coupling models is positive (at saturation density) so that the potential energy part of the symmetry energy at saturation density is also positive.

For $U_{\rm sym}^{\rm OPT}$, whether it increases or deceases with nucleon momentum depends on the isospin splitting of the nucleon scalar self energy (scalar potential) or Dirac mass in neutron-rich nuclear matter. This can be seen from Eq.(14) if it is re-expressed as

$$\begin{aligned} U_{\rm sym}^{\rm OPT} &= \frac{E_n-E_p}{2\alpha} \\ &= \frac{1}{2\alpha}(\Sigma_n^0-\Sigma_p^0+\sqrt{\vec{p}^2+(M_n+\Sigma_n^S)^2} \\ &\quad -\sqrt{\vec{p}^2+(M_p+\Sigma_p^S)^2}) \\ &= \frac{1}{2\alpha}[\Sigma_n^0-\Sigma_p^0+\sqrt{\vec{p}^2+(M^*_{{\rm Dirac},n})^2} \\ &\quad -\sqrt{\vec{p}^2+(M^*_{{\rm Dirac},p})^2}]. \end{aligned} \tag{113}$$

We note that $U_{\rm sym}^{\rm OPT}$ increases with momentum for the parameter sets HA, NL$\rho\delta$, DDRH-corr, and PC-F4 while

the opposite behavior is observed for the parameter sets PC-F2, PC-LA, and FKVW.

For the momentum dependence of $U_{\rm sym}^{\rm SOD}$, it is similar to that of $U_{\rm sym}^{\rm OPT}$ if we rewrite Eq. (16) as

$$U_{\rm sym}^{\rm SOD} = \frac{E_n - E_p - (M_\tau^2 + \vec{p}^2)(\frac{1}{E_n} - \frac{1}{E_n})}{4\alpha} = U_{\rm sym}^{\rm OPT}/2 - \frac{(M_\tau^2 + \vec{p}^2)(\frac{1}{E_n} - \frac{1}{E_n})}{4\alpha}. \quad (114)$$

In this case, $U_{\rm sym}^{\rm SOD}$ increases with nucleon momentum for the parameter sets HA, NL$\rho\delta$, and DDRH-corr while it decreases for other parameter sets considered here.

In Ref.[78], it has been argued that it is the "Schrödinger-equivalent potential " $U_{\rm SEP}$ (Eq. (10)) and thus its corresponding symmetry potential $U_{\rm sym}^{\rm SEP}$ that should be compared with the results from non-relativistic models. As discussed before, the experimental data indicate that the nuclear symmetry potential at nuclear matter saturation density, i.e., the Lane potential $U_{\rm Lane}$, clearly decreases at low energies (beam energy $E_{\rm kin}$ up to about 100 MeV and corresponding momentum values ranging from about 300 MeV/c to 470 MeV/c), which is obviously contradictory to the results for $U_{\rm sym}^{\rm SEP}$ from all of the 23 parameter sets considered here. On the other hand, $U_{\rm sym}^{\rm OPT}$ and $U_{\rm sym}^{\rm SOD}$ for some parameter sets can decrease with nucleon momentum, which is qualitatively consistent with experimental results.

For nucleons with momenta less than about $250 - 300$ MeV/c or $E_{\rm kin} < 0$, although observed increase of $U_{\rm sym}^{\rm SEP}$ with momentum for all 23 parameter sets, and $U_{\rm sym}^{\rm OPT}$ as well as $U_{\rm sym}^{\rm SOD}$ with some parameter sets, seems to be consistent with the results from the microscopic DBHF [17], the extended BHF with 3-body forces [24], and chiral perturbation theory calculations [88], i.e., the symmetry potential stays as a constant or slightly increases with momentum before decreasing at high momenta, it fails to describe the high momentum/energy behaviors of the nuclear symmetry potential extracted from nucleon-nucleus scattering experiments and (p,n) charge exchange reactions at beam energies up to about 100 MeV.

We note that in studies based on the relativistic impulse approximation with empirical NN scattering amplitude and the nuclear scalar and vector densities from the RMF model, the Schrödinger-equivalent nuclear symmetry potential at fixed baryon density is found to decrease with increasing nucleon energy in the range of $100 \leq E_{\rm kin} \leq 400$ MeV [92] and becomes essentially constant once the nucleon kinetic energy is greater than about 500 MeV [89].

C. Nucleon effective mass

For the different nucleon effective masses in symmetric nuclear matter at saturation density, we show in Table II the results from the 23 parameter sets in the nonlinear, density-dependent, and point-coupling RMF models. It is seen that the values of $M_{\rm Dirac}^*/M$, $M_{\rm Landau}^*/M$, $M_{\rm Lorentz}^*/M$, $M_{\rm OPT}^*/M$, and $M_{\rm SOD}^*/M$ are in the range of $0.55 \sim 0.75$, $0.62 \sim 0.80$, $0.64 \sim 0.80$, $0.60 \sim 0.77$, and $0.57 \sim 0.76$, respectively. The parameter sets NL2, HA, NLρ and NL$\rho\delta$ seem to give too large values, i.e., 0.67, 0.68, 0.75, and 0.75, respectively, for the $M_{\rm Dirac}^*/M$ as values in the range of $0.55 \sim 0.60$ are needed to describe reasonably the spin-orbit splitting in finite nuclei using the RMF models. On the other hand, the larger Dirac masses leads to larger Landau masses $M_{\rm Landau}^*/M$ of 0.72, 0.74, 0.80, and 0.80, respectively, for the parameter sets NL2, HA, NLρ and NL$\rho\delta$, which are consistent with the empirical constraint of $M^*{}_{\rm Landau}/M = 0.8 \pm 0.1$ [94, 95, 96, 97].

TABLE II: Values of different nucleon effective masses, i.e., $M_{\rm Dirac}^*/M$, $M_{\rm Landau}^*/M$, $M_{\rm Lorentz}^*/M$, $M_{\rm OPT}^*/M$, and $M_{\rm SOD}^*/M$ in symmetric nuclear matter at saturation density using the 23 parameter sets in the nonlinear, density-dependent, and point-coupling RMF models. The last column gives the references for corresponding parameter sets.

Model	$\frac{M^*_{Dirac}}{M}$	$\frac{M^*_{Landau}}{M}$	$\frac{M^*_{Lorentz}}{M}$	$\frac{M^*_{OPT}}{M}$	$\frac{M^*_{SOD}}{M}$	Ref.
NL1	0.57	0.64	0.65	0.61	0.59	[102]
NL2	0.67	0.72	0.74	0.70	0.68	[102]
NL3	0.60	0.66	0.67	0.63	0.61	[103]
NL-SH	0.60	0.66	0.67	0.63	0.61	[104]
TM1	0.63	0.69	0.71	0.67	0.65	[105]
PK1	0.61	0.66	0.68	0.64	0.62	[106]
FSUGold	0.61	0.67	0.69	0.65	0.62	[76]
HA	0.68	0.74	0.75	0.71	0.69	[107]
NLρ	0.75	0.80	0.82	0.77	0.76	[100]
NL$\rho\delta$	0.75	0.80	0.82	0.77	0.76	[100]
TW99	0.55	0.62	0.64	0.60	0.57	[46]
DD-ME1	0.58	0.64	0.66	0.62	0.59	[108]
DD-ME2	0.57	0.63	0.65	0.61	0.59	[109]
PKDD	0.57	0.63	0.65	0.61	0.59	[106]
DD	0.56	0.63	0.64	0.61	0.58	[93]
DD-F	0.56	0.62	0.64	0.60	0.57	[110]
DDRH-corr	0.55	0.63	0.64	0.60	0.58	[47]
PC-F1	0.61	0.67	0.69	0.64	0.62	[49]
PC-F2	0.61	0.67	0.69	0.64	0.62	[49]
PC-F3	0.61	0.67	0.69	0.64	0.62	[49]
PC-F4	0.61	0.67	0.69	0.64	0.62	[49]
PC-LA	0.58	0.64	0.65	0.61	0.59	[49]
FKVW	0.62	0.68	0.70	0.65	0.63	[53]

The density dependence of the different nucleon effective masses in symmetric nuclear matter and corresponding isospin splitting $(M_n^* - M_p^*)/M$ in asymmetric nuclear matter with isospin asymmetry $\alpha = 0.5$ are shown in Fig. 8 for the parameter sets NL1, NL2, NL3, NL-

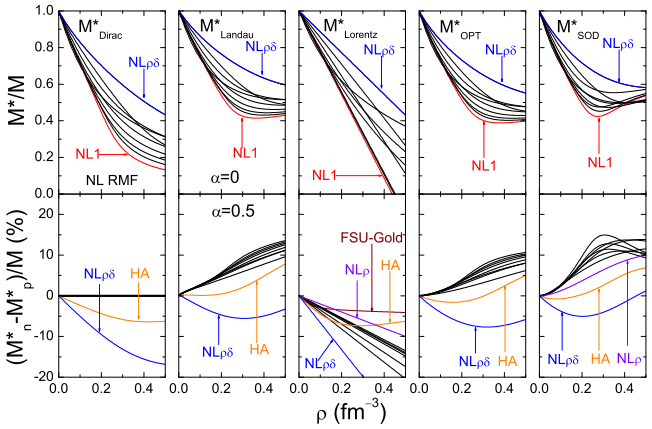

FIG. 8: (Color online) Density dependence of different nucleon effective masses, i.e., $M^*_{\rm Dirac}/M$, $M^*_{\rm Landau}/M$, $M^*_{\rm Lorentz}/M$, $M^*_{\rm OPT}/M$, and $M^*_{\rm SOD}/M$ in symmetric nuclear matter as well as their corresponding isospin splittings in neutron-rich nuclear matter with isospin asymmetry $\alpha = 0.5$ for the parameter sets NL1, NL2, NL3, NL-SH, TM1, PK1, FSU-Gold, HA, NLρ, and NL$\rho\delta$ in the nonlinear RMF model.

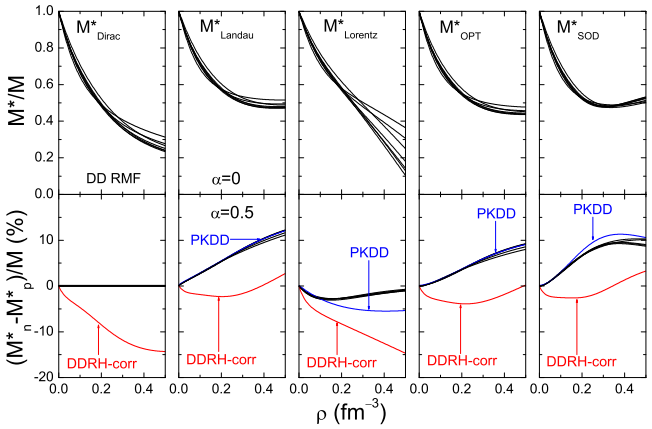

FIG. 9: (Color online) Same as Fig. 8 but for TW99, DD-ME1, DD-ME2, PKDD, DD, DD-F, and DDRH-corr in the density-dependent RMF model.

SH, TM1, PK1, FSU-Gold, HA, NLρ, and NL$\rho\delta$ in the nonlinear RMF model. Figs. 9 and 10 display the same results as in Fig. 8 but for the parameter sets TW99, DD-ME1, DD-ME2, PKDD, DD, DD-F, and DDRH-corr in the density-dependent RMF models and for PC-F1, PC-F2, PC-F3, PC-F4, PC-LA, and FKVW in the point-coupling RMF model, respectively. It is seen that different parameter sets in the nonlinear RMF model give significantly different density dependence for the nucleon effective masses while the different parameter sets in the density-dependent and point-coupling RMF models predict roughly the same density dependence for the nucleon effective masses except that the parameter set PC-LA gives very large values for the nucleon effective masses at high densities. This unusual behavior for PC-LA was also observed in Ref. [49], and it is due to the fact that

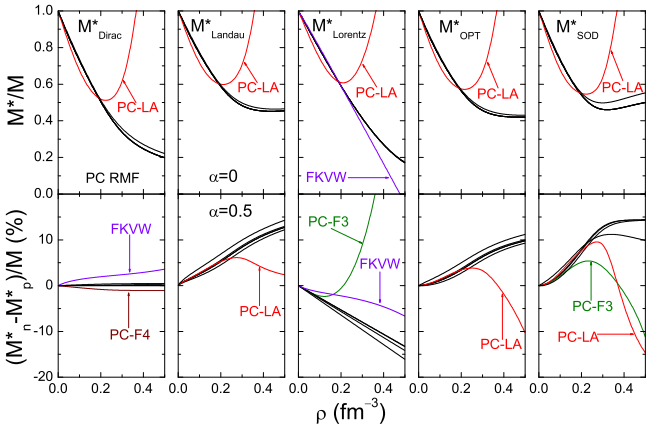

FIG. 10: (Color online) Same as Fig. 8 but for PC-F1, PC-F2, PC-F3, PC-F4, PC-LA, and FKVW in the point-coupling RMF model.

the coupling constant $\gamma_{\rm S}$ for the higher-order interaction term in PC-LA is positive [48] and dominates at high density, leading thus to the very large nucleon effective mass.

For the Landau mass at a fixed baryon density, its value $M^*_{\rm Landau}/M$ is generally larger than $M^*_{\rm Dirac}/M$. This can be seen from Eq. (18) if it is rewritten as

$$M^*_{{\rm Landau},\tau} = (E_\tau - \Sigma^0_\tau) = \sqrt{p^2_{F,\tau} + (M_\tau + \Sigma^S_\tau)^2} = \sqrt{p^2_{F,\tau} + M^{*2}_{{\rm Dirac},\tau}} \quad (115)$$

which shows that $M^*_{{\rm Landau},\tau} \geq M^*_{{\rm Dirac},\tau}$ if nucleon self-energies are independent of momentum/energy.

For the Lorentz mass $M^*_{\rm Lorentz}$, $M^*_{\rm Lorentz}/M$ depends almost linearly on density and thus has a stronger density dependence than the Dirac and Landau masses. We note from Eqs. (13) and (115) that Eq. (19) can be reduced to

$$M^*_{{\rm Lorentz},\tau} = M_\tau - \Sigma^0_\tau, \quad (116)$$

if nucleon self-energies are independent of momentum/energy. Therefore, the density dependence of $M^*_{\rm Lorentz}$ is determined uniquely by the density dependence of nucleon vector self-energy. In the nonlinear RMF model, most of the parameter sets, except for TM1, PK1 and FSU-Gold which include the self-coupling of the ω meson field, give a linear density dependence for Σ^0_τ, leading thus to the observed linear density dependence of $M^*_{\rm Lorentz}$. As to the nonlinear density dependence of $M^*_{\rm Lorentz}$ in the density-dependent RMF model and point-coupling models, it is due to the nonlinear density dependence of the coupling constant or the inclusion of higher-order couplings.

For $M^*_{\rm OPT}/M$ and $M^*_{\rm SOD}/M$, they are seen to have roughly same magnitude and also same density dependence as $M^*_{\rm Landau}/M$. This feature can be understood from the fact that with the dispersion relation of Eq.

(13), Eq. (20) and Eq. (21) can be re-expressed as

$$M^*_{\rm OPT,\tau} = \frac{M_\tau}{\sqrt{p^2_{F,\tau}+M^2_\tau}} M^*_{\rm Landau,\tau} \tag{117}$$

and

$$M^*_{\rm SOD,\tau} = M_\tau \left[\frac{M^*_{\rm Landau,\tau}}{E_\tau} + \frac{E^2_\tau - (p^2_{F,\tau}+M^2_\tau)}{2E^2_\tau} \right], \tag{118}$$

respectively. Since $p^2_{F,\tau} \ll M^2_\tau$ (For example, $p_F \approx 385$ MeV/c at $\rho_B = 0.5$ fm^{-3}), we have $M_\tau/\sqrt{p^2_{F,\tau}+M^2_\tau} \approx 1$ (with an error of a few percent) and thus $M^*_{\rm OPT,\tau} \approx M^*_{\rm Landau,\tau}$. Furthermore, the second term in Eq. (118) can be neglected compared with the first term as $M_\tau/E_\tau \sim 1$ (it is a good approximation at low densities and with an error of about 20% at high densities, e.g., $\rho_B = 0.5$ fm^{-3}). As a result, we have $M^*_{\rm SOD,\tau} \sim M^*_{\rm Landau,\tau}$.

From the Dirac equation, one sees that condensed scalar fields (scalar self-energies) lead to a shift of nucleon mass such that the nuclear matter is described as a system of pseudo-nucleons with masses M^* (Dirac mass) moving in classical vector fields with δ meson field or isovector-scalar potential further generating the splitting of the proton and neutron Dirac masses in asymmetric nuclear matter. For the isospin splitting of $M^*_{\rm Dirac}$ in neutron-rich nuclear matter, it is interesting to see that the parameter sets HA, NL$\rho\delta$, DDRH-corr, and PC-F4 give $M^*_{\rm Dirac,p} > M^*_{\rm Dirac,n}$ while PC-F2, PC-LA, and FKVW exhibit the opposite behavior of $M^*_{\rm Dirac,p} < M^*_{\rm Dirac,n}$. This feature implies that the isospin-dependent scalar potential can be negative or positive depending on the parameter sets used. In the nonlinear RMF model, we obtain from Eqs. (32) and (37)

$$M^*_{\rm Dirac,n} - M^*_{\rm Dirac,p} = -2\left(\frac{g_\delta}{m_\delta}\right)^2 (\rho_{S,n} - \rho_{S,p}), \tag{119}$$

which indicates that we always have $M^*_{\rm Dirac,p} > M^*_{\rm Dirac,n}$ in the neutron-rich nuclear matter where $\rho_{S,n} > \rho_{S,p}$. This argument is also applicable to the density-dependent RMF model by replacing g_δ with the density dependent Γ_δ. For the nonlinear point-coupling models, we have, on the other hand,

$$M^*_{\rm Dirac,n} - M^*_{\rm Dirac,p} = 2\alpha_{\rm TS}(\rho_{S,n} - \rho_{S,p}). \tag{120}$$

A similar equation can be obtained for the density-dependent point-coupling models with the replacement of $\alpha_{\rm TS}$ by the density dependent G_{TS}. Therefore, the isospin splitting of $M^*_{\rm Dirac}$ in neutron-rich nuclear matter depends on the sign of the isovector-scalar coupling constant $\alpha_{\rm TS}$ and G_{TS} in the point-coupling models. Since the value of $\alpha_{\rm TS}$ in PC-F2 and PC-LA as well as the value of G_{TS} in FKVW are positive, these parameter sets lead to the isospin-splitting $M^*_{\rm Dirac,n} > M^*_{\rm Dirac,p}$ in neutron-rich nuclear matter, which is opposite to that in other parameter sets considered here. The isospin splitting of $M^*_{\rm Dirac}$ is directly related to the isovector spin-orbit potential that determines the isospin-dependent spin-orbit splitting in finite nuclei. Unfortunately, there are no clear experimental indication about the isospin dependence of the spin-orbit splitting in finite nuclei [47], so detailed experimental data on the single-particle energy levels in exotic nuclei are needed to pin down the isospin splitting of $M^*_{\rm Dirac}$ in asymmetric nuclear matter.

For the isospin splitting of $M^*_{\rm Landau}$ in neutron-rich nuclear matter, most parameter sets give $M^*_{\rm Landau,n} > M^*_{\rm Landau,p}$, which is consistent with the usual results in non-relativistic models. The parameter sets NL$\rho\delta$ and DDRH-corr give, however, the opposite result due to the strong isospin-splitting of $M^*_{\rm Dirac}$ with $M^*_{\rm Dirac,n} < M^*_{\rm Dirac,p}$ for NL$\rho\delta$ and DDRH-corr and the fact that $M^*_{\rm Landau}$ is related to the Fermi momentum and $M^*_{\rm Dirac}$ according to Eq. (115). The isospin-splitting $M^*_{\rm Landau,n} > M^*_{\rm Landau,p}$ implies that neutrons have a larger level density at the Fermi energy and thus more compressed single-particle levels in finite nuclei than protons.

For the isospin splitting of $M^*_{\rm Lorentz}$ in neutron-rich nuclear matter, all parameter sets give $M^*_{\rm Lorentz,p} > M^*_{\rm Lorentz,n}$ except that the PC-L3 gives $M^*_{\rm Lorentz,p} < M^*_{\rm Lorentz,n}$ at high densities. From Eq. (116), we have

$$M^*_{\rm Lorentz,n} - M^*_{\rm Lorentz,p} = -(\Sigma^0_n - \Sigma^0_p), \tag{121}$$

which leads to the observed isospin-splitting $M^*_{\rm Lorentz,p} > M^*_{\rm Lorentz,n}$ as we generally have $\Sigma^0_n > \Sigma^0_p$ as discussed above. For the parameter set PC-L3, it includes a higher-order isovector-vector term through the parameter $\gamma_{\rm TV}$. Since the latter has a negative value and dominates at high densities according to Eq. (82), it leads to $\Sigma^0_n < \Sigma^0_p$ and thus $M^*_{\rm Lorentz,p} < M^*_{\rm Lorentz,n}$ at high densities. The isospin splitting of $M^*_{\rm OPT}/M$ and $M^*_{\rm SOD}/M$ in neutron-rich nuclear matter show a similar behavior as $M^*_{\rm Landau}$ as expected from the discussions below Eqs. (117) and (118).

D. Nucleon scalar density

The nucleon scalar density as defined in Eq. (34) is the source for the nucleon scalar self-energy (scalar potential). In the RMF model, the isospin-dependent nucleon scalar density is uniquely related to the nucleon Dirac mass as shown in Eq. (35). The latter equation also shows that the scalar density is less than the baryon density due to the factor $M^*_i/\sqrt{\vec{k}^2+(M^*_i)^2}$ which causes a reduction of the contribution of rapidly moving nucleons to the scalar source term. This mechanism is responsible for nuclear matter saturation in the mean-field theory and essentially distinguishes relativistic models from non-relativistic ones. In practice, the isospin-dependent nucleon scalar density is also an essential ingredient for evaluating the relativistic optical potential for neutrons and

protons in the relativistic impulse approximation (See, e.g., Refs. [89, 92] and references therein).

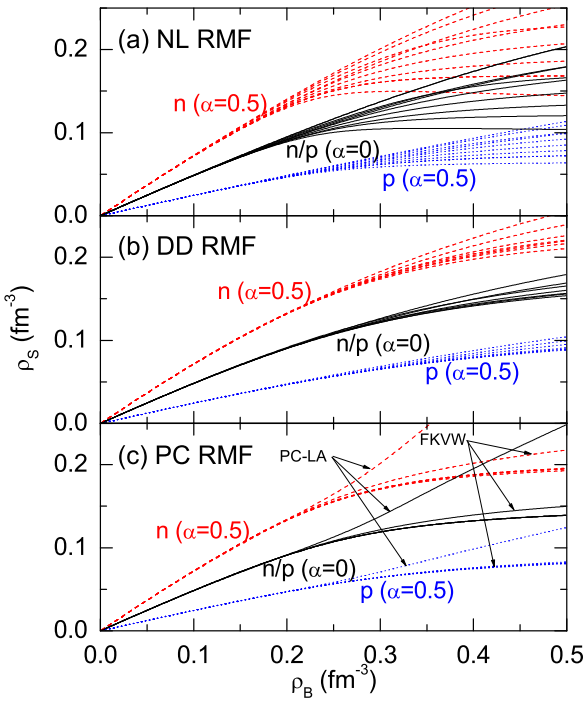

FIG. 11: (Color online) Neutron and proton scalar densities as functions of baryon density in nuclear matter with isospin asymmetry $\alpha = 0$ and 0.5 for the parameter sets NL1, NL2, NL3, NL-SH, TM1, PK1, FSU-Gold, HA, NLρ, and NL$\rho\delta$ of the nonlinear RMF model (a); TW99, DD-ME1, DD-ME2, PKDD, DD, DD-F, and DDRH-corr of the density-dependent RMF model (b); PC-F1, PC-F2, PC-F3, PC-F4, PC-LA, and FKVW of the point-coupling RMF model (c).

In Fig. 11, we show the neutron and proton scalar densities as functions of the baryon density ρ_B in nuclear matter with isospin asymmetry $\alpha = 0$ and 0.5 for the 23 parameter sets from the nonlinear, density-dependent, and point-coupling RMF models. It is seen that the neutron scalar density is larger than that of protons in neutron-rich nuclear matter at a fixed baryon density. Although results for different parameter sets are almost the same at lower baryon densities, they become different when $\rho_B \gtrsim 0.25$ fm^{-3}, and this is consistent with the conclusions of Refs. [89, 92]. In particular, different parameter sets in the nonlinear RMF model predict a larger uncertainty for the value of the nucleon scalar density at high baryon density while all the parameter sets (except PC-LA) in the density-dependent RMF model and point-coupling models give roughly same results for the nucleon scalar density. These features are consistent with the results for the density dependence of nucleon Dirac mass shown in Figs. 8, 9, and 10. At low baryon densities, neutron and proton scalar densities are seen to increase roughly linearly with baryon density, and this can be easily understood from Eq. (35), which is reduced to the following expression at low densities ($|\vec{k}| \to 0$ due to $k_F \to 0$):

$$\rho_{S,i} \approx \frac{2}{(2\pi)^3}\int_0^{k_F^i} d^3k\,\frac{M_i^*}{M_i^*} = \frac{2}{(2\pi)^3}\int_0^{k_F^i} d^3k = \rho_{B,i},\ i = p, n. \quad (122)$$

Therefore, neutron and proton scalar densities generally approach their respective baryon densities in asymmetric nuclear matter at low baryon densities.

V. SUMMARY AND CONCLUSIONS

Using different versions of relativistic mean-field models that are commonly used in current nuclear structure studies, i.e., the nonlinear model, the model with density-dependent nucleon-meson coupling, and the point-coupling model, we have investigated systematically the isospin-dependent bulk and single-particle properties of isospin-asymmetric nuclear matter. In particular, we considered 23 parameter sets commonly and successfully used in nuclear structure studies, i.e., NL1, NL2, NL3, NL-SH, TM1, PK1, FSU-Gold, HA, NLρ, NL$\rho\delta$ for the nonlinear RMF model; TW99, DD-ME1, DD-ME2, PKDD, DD, DD-F, and DDRH-corr for the density-dependent RMF model; and PC-F1, PC-F2, PC-F3, PC-F4, PC-LA, and FKVW for the point-coupling RMF model. Most of the parameter sets are obtained from fitting the binding energies and charge radii of a large number of nuclei in the periodic table or the results from the microscopic DBHF approach, which have been shown to describe successfully a number of the properties of finite nuclei.

Using these models, we have studied the density dependence of nuclear symmetry energy and compared the results with the symmetry energy recently extracted from the analyses of the isospin diffusion data from heavy-ion collisions based on an isospin- and momentum-dependent transport model with in-medium NN cross sections, the isoscaling analyses of isotope ratios in intermediate energy heavy ion collisions, and measured isotopic dependence of the giant monopole resonances in even-A Sn isotopes. These analyses have led to the extraction of $L = 88 \pm 25$ MeV for the slope parameter of the nuclear symmetry energy at saturation density and $K_{\rm asy} = -500 \pm 50$ MeV or -550 ± 100 MeV for the isospin-dependent part of the isobaric incompressibility of isospin asymmetric nuclear matter, which may represent the most stringent phenomenological constraints available so far on the nuclear symmetry energy at subsaturation densities. Using these constraints, we have found that, among the 23 parameter sets considered in the present work, only six sets, i.e., TM1, NLρ, NL$\rho\delta$, PKDD, PC-LA, and FKVW, have nuclear symmetry energies that are consistent with the extracted L value of

88 ± 25 MeV while fifteen sets, i.e., NL3, NL-SH, TM1, PK1, HA, NLρ, NL$\rho\delta$, TW99, PKDD, DD-F, PC-F1, PC-F2, PC-F3, PC-F4, and FKVW, have nuclear symmetry energies that are consistent with the extracted $K_{\rm asy}$ value of -500 ± 50 MeV or -550 ± 100 MeV. Furthermore, we have found surprisingly that only five parameter sets, i.e., TM1, NLρ, NL$\rho\delta$, PKDD, and FKVW, in the 23 parameter sets have nuclear symmetry energies that are consistent with the extracted values for both L and $K_{\rm asy}$. We have noted that most parameter sets in the nonlinear and point-coupling RMF models predict stiffer symmetry energies while those in the density-dependent RMF model give softer symmetry energies. These features are probably related to the rather limited flexibility in the parametrization of the isovector channel in all RMF models and also the fact that most of the parameter sets are obtained from fitting properties of finite nuclei which are mostly near the β-stability line and thus have less constraint on the isospin-dependent properties of asymmetric nuclear matter. Moreover, we have focused here on the behavior of the symmetry energy around saturation density while the parameter sets in RMF models are fitted to the properties of finite nuclei that are more sensitive to the properties of the nuclear symmetry energy at sub-saturation densities.

We have also investigated the energy dependence of three different nucleon optical potentials, i.e., the "Schrö dinger-equivalent potential" $U_{\rm SEP}$ (Eq. (10)), the optical potential from the difference between the total energy of a nucleon in nuclear medium and its energy at the same momentum in free space $U_{\rm OPT}$ (Eq. (12)), and the optical potential based on the second-order Dirac equation $U_{\rm SOD}$ (Eq. (15)), as well as their corresponding symmetry potentials $U_{\rm sym}^{\rm SEP}$, $U_{\rm sym}^{\rm OPT}$, and $U_{\rm sym}^{\rm SOD}$ as functions of momentum. The results indicate that different optical potentials in symmetric nuclear matter exhibit similar energy dependence at low energies but have different high energy behaviors. In particular, at high energies, $U_{\rm SEP}$ continues to increase linearly with momentum while $U_{\rm OPT}$ and $U_{\rm SOD}$ seem to saturate and thus display a more satisfactory high-energy limit compared to the optical potentials extracted from proton-nucleus scatterings using the Dirac phenomenology. On the other hand, the nuclear symmetry potential at a fixed baryon density can increase or decrease with increasing nucleon momentum depending on the definition for the nucleon optical potential and the interactions used. For $U_{\rm sym}^{\rm SEP}$ at $\rho_B = 0.16$ fm^{-3}, results from all 23 parameter sets show that it increases with momentum, which is consistent with the predictions of microscopic DBHF and chiral perturbation calculations at low momenta (less than about 300 MeV/c) but is inconsistent with the experimental result that the nuclear symmetry potential at saturation density (the Lane potential $U_{\rm Lane}$) decreases at low energies (beam energy $E_{\rm kin}$ above 0 MeV and less than about 100 MeV and corresponding momentum values are from about 300 MeV/c to 470 MeV/c) and RIA predictions at higher energies. For $U_{\rm sym}^{\rm OPT}$ and $U_{\rm sym}^{\rm SOD}$, they can, however, decrease with momentum for some parameter sets, which is qualitatively consistent with the experimental constraint. Again, we emphasize that, for the three definitions of the optical potential and thus their corresponding nuclear symmetry potentials, only $U_{{\rm SEP},\tau}$ is well-defined theoretically and is Schrödinger-equivalent while $U_{{\rm OPT},\tau}$ and $U_{{\rm SOD},\tau}$ are used here for references as $U_{{\rm OPT},\tau}$ has been extensively used in microscopic DBHF calculations [80] and transport models for heavy-ion collisions [81] and $U_{{\rm SOD},\tau}$ has been used in analyses of the relativistic optical potential based on the Dirac phenomenology [82].

We have further explored different nucleon effective masses, i.e., $M^*_{\rm Dirac}$, $M^*_{\rm Landau}$, $M^*_{\rm Lorentz}$, $M^*_{\rm OPT}$, and $M^*_{\rm SOD}$ in symmetric nuclear matter as well as their isospin-splittings in neutron-rich nuclear matter. Most of the parameter sets are found to give reasonable values for $M^*_{\rm Dirac}$ as required by the spin-orbit splitting data in finite nuclei but too small values for $M^*_{\rm Landau}$, implying that they would give too small a level density at the Fermi energy and too large a spread of the single-particle levels in finite nuclei. For $M^*_{\rm Lorentz}$, it is found to display the strongest (almost linear) density dependence even at high densities. Interestingly, including the isovector-scalar channel leads to the isospin-splitting of $M^*_{\rm Dirac}$, and $M^*_{{\rm Dirac},n} > M^*_{{\rm Dirac},p}$ is always obtained in neutron-rich nuclear matter for the nonlinear and density-dependent RMF models but an opposite result can be observed in the point-coupling model. For $M^*_{\rm Landau}$, most parameter sets give the isospin splitting $M^*_{{\rm Landau},n} > M^*_{{\rm Landau},p}$ in neutron-rich nuclear matter, which is consistent with usual results in non-relativistic models, while an opposite isospin-splitting is observed for $M^*_{\rm Lorentz}$. In addition, $M^*_{\rm OPT}$, and $M^*_{\rm SOD}$ are found to display similar behaviors as $M^*_{\rm Landau}$.

Finally, we have studied the baryon density dependence of the nucleon scalar density and its isospin-splitting in neutron-rich nuclear matter. The results indicate that the neutron scalar density is larger than that of proton in neutron-rich nuclear matter at a fixed baryon density. At low baryon densities, the neutron and proton scalar densities generally approach their respective baryon densities in asymmetric nuclear matter.

In the present work, we have focused on three versions of standard RMF models, i.e., the nonlinear, density-dependent, and point-coupling RMF models. We note that there are some recent works [115, 116, 117, 118, 119] in which the standard RMF models are extended to include density-dependent hadron masses and meson coupling constants via the Brown-Rho (BR) scaling [120]. In particular, the parameter sets SLC and SLCd constructed in Ref. [117, 118] are not only consistent with current experimental results for symmetric matter at normal and supra-normal densities and the symmetry energy constrained by the isospin diffusion data at sub-saturation densities, but also give a fairly satisfactory description of the ground state properties of finite nuclei, including binding energies, charge radii, and neutron skin

thickness.

In all standard RMF models, the nucleon self-energies are independent of momentum/energy. As a result, the Dirac mass and the Landau mass obtained from these models cannot be simultaneously consistent with experimental data (see, e.g., Eq. (115)). Also, the "Schrödinger-equivalent potential" $U_{\rm SEP}$ (Eq. (10)) in these models increases linearly with nucleon energy even at high energies. Recently, momentum-dependent nucleon self-energies have been introduced in the RMF model by including in the Lagrangian density the couplings of meson fields to the derivatives of nucleon densities [93, 121], and the results indicate that a reasonable energy dependence of the "Schrödinger-equivalent potential" in symmetric nuclear matter at saturation density can be obtained, and the Landau mass can also be increased to a more reasonable value while keeping the Dirac mass unchanged, which further leads to an improved description of β-decay half-lives of neutron-rich nuclei in the $Z \approx 28$ and $Z \approx 50$ regions [94]. In the framework of density-functional theory, including the couplings of meson fields to the derivatives of nucleon densities in the Lagrangian density provides an effective way to take into account higher-order effects. Another way to introduce the momentum-dependence in nucleon self-energies is to include the Fock exchange terms by means of the relativistic Hartree-Fock (RHF) approximation, even though in practice the inclusion of the Fock terms would increase significantly the numerical complexity such that it is very difficult to find appropriate effective Lagrangians for the RHF model to give satisfactory quantitative description of the nuclear structure properties compared with standard RMF models [73, 122, 123, 124, 125, 126, 127, 128, 129, 130, 131]. Recently, there have been some developments in the density-dependent RHF approach [132, 133, 134]. It is shown that the density-dependent RHF model can describe the properties of both finite nuclei and nuclear matter with results comparable to those from standard RMF models. A more phenomenological way to improve the results of RMF models is to introduce momentum- as well as isospin-dependent form factors in the meson-nucleon coupling constants. It has been shown in Refs. [135, 136, 137] that the empirically observed energy dependence of the nuclear optical potential in symmetric nuclear matter at saturation density can be reproduced by relativistic mean-field models with momentum-dependent form factors. Finally, to better understand the isospin-dependent properties of asymmetric nuclear matter it is crucial to investigate the density and momentum dependence of underlying isovector nuclear effective interaction. To reach this ultimate goal, we need not only more advanced theoretical approaches but also more experimental data both on finite nuclei, especially those far from β-stability line, and from heavy-ion reactions induced by high energy neutron-rich nuclei.

Acknowledgments

We would like to thank Paolo Finelli, Wei-Zhou Jiang, Plamen G. Krastev, and Gao-Chan Yong for helpful discussions or communications. L.W.C. also thanks the hospitality of Texas A&M University at Commerce and College Station where part of the work was done. This work was supported in part by the National Natural Science Foundation of China under Grant Nos. 10575071 and 10675082, MOE of China under project NCET-05-0392, Shanghai Rising-Star Program under Grant No. 06QA14024, the SRF for ROCS, SEM of China, the China Major State Basic Research Development Program under Contract No. 2007CB815004 (L.W.C.), the US National Science Foundation under Grant No. PHY-0457265, the Welch Foundation under Grant No. A-1358 (C.M.K.), the US National Science Foundation under Grant No. PHY-0652548, and the Research Corporation under Award No. 7123 (B.A.L.).

APPENDIX A: ISOSPIN- AND MOMENTUM-DEPENDENT MDI INTERACTION

The isospin- and momentum-dependent MDI interaction is based on a modified finite-range Gogny effective interaction [25]. In the MDI interaction, the potential energy density $V(\rho,\alpha)$ of an asymmetric nuclear matter at total density ρ and isospin asymmetry α is expressed as follows [25, 55],

$$\begin{aligned} V(\rho,\alpha) &= \frac{A_u\rho_n\rho_p}{\rho_0}+\frac{A_l}{2\rho_0}(\rho_n^2+\rho_p^2)+\frac{B}{\sigma+1}\frac{\rho^{\sigma+1}}{\rho_0^\sigma} \\ &\times (1-x\alpha^2)+\frac{1}{\rho_0}\sum_{\tau,\tau'}C_{\tau,\tau'} \\ &\times \int\int d^3p d^3p' \frac{f_\tau(\vec{r},\vec{p})f_{\tau'}(\vec{r},\vec{p}')}{1+(\vec{p}-\vec{p}')^2/\Lambda^2}. \end{aligned} \tag{A1}$$

In the mean-field approximation, Eq. (A1) leads to the following single-particle potential for a nucleon with momentum $\vec{p}$ and isospin τ in asymmetric nuclear matter [25, 55]:

$$\begin{aligned} U(\rho,\alpha,\vec{p},\tau) &= A_u(x)\frac{\rho_{-\tau}}{\rho_0}+A_l(x)\frac{\rho_\tau}{\rho_0} \\ &+ B(\frac{\rho}{\rho_0})^\sigma(1-x\alpha^2)-8\tau x\frac{B}{\sigma+1}\frac{\rho^{\sigma-1}}{\rho_0^\sigma}\alpha\rho_{-\tau} \\ &+ \frac{2C_{\tau,\tau}}{\rho_0}\int d^3p'\frac{f_\tau(\vec{r},\vec{p}')}{1+(\vec{p}-\vec{p}')^2/\Lambda^2} \\ &+ \frac{2C_{\tau,-\tau}}{\rho_0}\int d^3p'\frac{f_{-\tau}(\vec{r},\vec{p}')}{1+(\vec{p}-\vec{p}')^2/\Lambda^2}. \end{aligned} \tag{A2}$$

In the above $\tau = 1/2$ $(-1/2)$ for neutrons (protons); $\sigma = 4/3$; $f_\tau(\vec{r},\vec{p})$ is the phase-space distribution function at coordinate $\vec{r}$ and momentum $\vec{p}$. The parameters $A_u(x), A_l(x), B, C_{\tau,\tau}, C_{\tau,-\tau}$ and Λ are obtained by fitting

the momentum-dependence of $U(\rho,\alpha,\vec{p},\tau)$ to that predicted by the Gogny Hartree-Fock and/or the Brueckner-Hartree-Fock calculations, the saturation properties of symmetric nuclear matter and the symmetry energy of 31.6 MeV at normal nuclear matter density $\rho_0 = 0.16$ fm^{-3} [25]. The incompressibility K_0 of cold symmetric nuclear matter at saturation density ρ_0 is set to be 211 MeV. The parameters $A_u(x)$ and $A_l(x)$ depend on the x parameter according to

$$A_u(x) = -95.98 - x\frac{2B}{\sigma+1},\ A_l(x) = -120.57 + x\frac{2B}{\sigma+1}. \tag{A3}$$

The different x values in the MDI interaction are introduced to vary the density dependence of the nuclear symmetry energy while keeping other properties of the nuclear equation of state fixed [55], and they can be adjusted to mimic the predictions of microscopic and/or phenomenological many-body theories on the density dependence of nuclear matter symmetry energy. The last two terms in Eq. (A2) contain the momentum-dependence of the single-particle potential. The momentum dependence of the symmetry potential stems from the different interaction strength parameters $C_{\tau,-\tau}$ and $C_{\tau,\tau}$ for a nucleon of isospin τ interacting, respectively, with unlike and like nucleons in the background fields. More specifically, we use $C_{\tau,-\tau} = -103.4$ MeV and $C_{\tau,\tau} = -11.7$ MeV.

With $f_\tau(\vec{r},\vec{p}) = \frac{2}{h^3}\Theta(p_f(\tau)-p)$ for nuclear matter at zero temperature, the integrals in Eqs. (A1) and (A2) can be calculated analytically and we find

$$\begin{aligned}
&\int\int d^3p d^3p' \frac{f_\tau(\vec{r},\vec{p}) f_{\tau'}(\vec{r},\vec{p}')}{1+(\vec{p}-\vec{p}')^2/\Lambda^2} \\
&= \frac{1}{6}\left(\frac{4\pi}{h^3}\right)^2 \Lambda^2 \left\{ p_f(\tau)p_f(\tau')\left[3(p_f^2(\tau)+p_f^2(\tau')) - \Lambda^2\right]\right. \\
&\quad +4\Lambda\left[(p_f^3(\tau)-p_f^3(\tau'))\tan^{-1}\frac{p_f(\tau)-p_f(\tau')}{\Lambda} - (p_f^3(\tau)+p_f^3(\tau'))\tan^{-1}\frac{p_f(\tau)+p_f(\tau')}{\Lambda}\right] \\
&\quad \left.+\frac{1}{4}\left[\Lambda^4 + 6\Lambda^2(p_f^2(\tau)+p_f^2(\tau')) - 3(p_f^2(\tau)-p_f^2(\tau'))^2\right]\ln\frac{(p_f(\tau)+p_f(\tau'))^2+\Lambda^2}{(p_f(\tau)-p_f(\tau'))^2+\Lambda^2}\right\}
\end{aligned} \tag{A4}$$

and

$$\begin{aligned}
&\int d^3p' \frac{f_\tau(\vec{r},\vec{p}')}{1+(\vec{p}-\vec{p}')^2/\Lambda^2} \\
&= \frac{2}{h^3}\pi\Lambda^3\left[\frac{p_f^2(\tau)+\Lambda^2-p^2}{2p\Lambda}\ln\frac{(p+p_f(\tau))^2+\Lambda^2}{(p-p_f(\tau))^2+\Lambda^2} + \frac{2p_f(\tau)}{\Lambda} - 2\tan^{-1}\frac{p+p_f(\tau)}{\Lambda} - 2\tan^{-1}\frac{p-p_f(\tau)}{\Lambda}\right].
\end{aligned} \tag{A5}$$

With above results as well as the well-known contribution from nucleon kinetic energies in free Fermi gas model, we can thus easily obtain the EOS of asymmetric nuclear matter at zero temperature.

We note that the MDI interaction has been extensively used in the transport model for studying isospin effects in intermediate energy heavy-ion collisions induced by neutron-rich nuclei [26, 28, 55, 138, 139, 140, 141, 142, 143] and the study of the thermal properties of asymmetric nuclear matter [144, 145]. In particular, the isospin diffusion data from NSCL/MSU have constrained the value of x to between 0 and -1 for nuclear matter densities less than about $1.2\rho_0$ [55, 56].

[1] W. Zhan *et al.*, Int. Jour. Mod. Phys. E **15**, 1941 (2006); http://www.impcas.ac.cn/zhuye/en/htm/247.htm.
[2] Y. Yano, "The RIKEN RI Beam Factory Project: A status report": Nucl. Instr. Meth. **B261**, 1009 (2007).
[3] See, e.g., http://www.gsi.de/fair/index_e.html.
[4] See, e.g., http://ganinfo.in2p3.fr/research/developments /spiral2.
[5] See, e.g.,Whitepapers of the 2007 NSAC Long Range Plan Town Meeting, Jan., 2007, Chicago, http://dnp.aps.org.
[6] B.A. Li, C.M. Ko, and W. Bauer, topical review, Int. Jour. Mod. Phys. E **7**, 147 (1998).
[7] Isospin Physics in Heavy-Ion Collisions at Intermediate Energies, Eds. Bao-An Li and W. Udo Schröder (Nova Science Publishers, Inc, New York, 2001).

[8] P. Danielewicz, R. Lacey, and W.G. Lynch, Science **298**, 1592 (2002).
[9] J.M. Lattimer and M. Prakash, Phys. Rep. **333**, 121 (2000).
[10] J.M. Lattimer and M. Prakash, Astrophys. J. **550**, 426 (2001).
[11] J.M. Lattimer and M. Prakash, Science **304**, 536 (2004).
[12] V. Baran, M. Colonna, V. Greco, and M. Di Toro, Phys. Rep. **410**, 335 (2005).
[13] A.W. Steiner, M. Prakash, J.M. Lattimer, and P.J. Ellis, Phys. Rep. **411**, 325 (2005).
[14] W.D. Myers and W.J. Swiatecki, Nucl. Phys. **A81**, 1 (1966).
[15] K. Pomorski and J. Dudek, Phys. Rev. C **67**, 044316 (2003).
[16] S. Ulrych and H. Müther, Phys. Rev. C **56**, 1788 (1997).
[17] E.N.E. van Dalen, C. Fuchs and A. Faessler, Nucl. Phys. **A741**, 227 (2004).
[18] Z.Y. Ma, J. Rong, B.Q. Chen, Z.Y. Zhu and H.Q. Song, Phys. Lett. **B604**, 170 (2004).
[19] F. Sammarruca, W. Barredo and P. Krastev, Phys. Rev. C **71**, 064306 (2005).
[20] E.N.E. van Dalen, C. Fuchs, and A. Faessler, Phys. Rev. Lett. **95**, 022302 (2005).
[21] E.N.E. van Dalen, C. Fuchs, and A. Faessler, Phys. Rev. C **72**, 065803 (2005).
[22] J. Rong, Z.Y. Ma, and N. Van Giai, Phys. Rev. C **73**, 014614 (2006).
[23] I. Bombaci and U. Lombardo, Phys. Rev. C **44**, 1892 (1991).
[24] W. Zuo, L.G. Cao, B.A. Li, U. Lombardo, and C.W. Shen, Phys. Rev. C **72**, 014005 (2005).
[25] C.B. Das, S. Das Gupta, C. Gale, and B.A. Li, Phys. Rev. C **67**, 034611 (2003).
[26] B.A. Li, C. B. Das, S. Das Gupta, and C. Gale, Phys. Rev. C **69**, 011603(R) (2004); Nucl. Phys. **A735**, 563 (2004).
[27] B.A. Li, Phys. Rev. C **69**, 064602 (2004).
[28] L.W. Chen, C.M. Ko, and B.A. Li, Phys. Rev. C **69**, 054606 (2004) [arXiv:nucl-th/0403049].
[29] J. Rizzo, M. Colonna, M. Di Toro, and V. Greco, Nucl. Phys. **A732**, 202 (2004).
[30] B. Behera, T.R. Routray, A. Pradhan, S.K. Patra, and P.K. Sahu, Nucl. Phys. **A753**, 367 (2005).
[31] J. Rizzo, M. Colonna, and M. Di Toro, Phys. Rev. C **72**, 064609 (2005).
[32] I. Bombaci, in [7], p.35.
[33] S. Shlomo and D. H. Youngblood, Phys. Rev. C **47**, 529 (1993).
[34] D.H. Youngblood, H.L. Clark, and Y.-W. Lui, Phys. Rev. Lett. **82**, 691 (1999).
[35] J.D.Walecka, Ann. Phys. (NY) **83**, 491 (1974).
[36] B.D. Serot and J.D. Walecka, Adv. Nucl. Phys. **16**, 1 (1986).
[37] P.-G. Reinhard, Rep. Prog. Phys. **52**, 439 (1989).
[38] P. Ring, Prog. Part. Nucl. Phys. **37**, 193 (1996).
[39] B.D. Serot and J.D. Walecka, Int. J. Mod. Phys. E **6**, 515 (1997).
[40] M. Bender, P.-H. Heenen, P.-G. Reinhard, Rev. Mod. Phys. **75**, 121 (2003).
[41] R.J. Furnstahl, Lect. Notes Phys. **641**, 1 (2004).
[42] J. Meng, H. Toki, S.G. Zhoub, S.Q. Zhang, W.H. Long, L.S. Geng, Prog. Part. Nucl. Phys. **57**, 470 (2006).
[43] H. Lenske and C. Fuchs, Phys. Lett. **B345**, 355 (1995).
[44] C. Fuchs, H. Lenske, and H. H. Wolter, Phys. Rev. C **52**, 3043 (1995).
[45] H. Shen,Y. Sugahara, andH. Toki, Phys. Rev. C **55**, 1211 (1997).
[46] S. Typel and H. H. Wolter, Nucl. Phys. **A656**, 331 (1999).
[47] F. Hofmann, C. M.Keil, and H. Lenske, Phys. Rev. C **64**, 034314 (2001).
[48] B.A. Nikolaus, T. Hoch, and D.G. Madland, Phys. Rev. C **46**, 1757 (1992).
[49] T. Bürvenich1, D.G. Madland, J.A. Maruhn1, and P.-G. Reinhard, Phys. Rev. C **65**, 044308 (2002).
[50] D.G. Madland, T. Bürvenich1, J.A. Maruhn1, and P.-G. Reinhard, Nucl. Phys. **A741**, 52 (2004).
[51] T. Bürvenich1, D.G. Madland, and P.-G. Reinhard, Nucl. Phys. **A744**, 92 (2004).
[52] P. Finelli, N. Kaiser, D. Vretenar and W. Weise, Nucl. Phys. **A435**, 449 (2004).
[53] P. Finelli, N. Kaiser, D. Vretenar and W. Weise, Nucl. Phys. **A770**, 1 (2006).
[54] M.B. Tsang et al., Phys. Rev. Lett. **92**, 062701 (2004).
[55] L.W. Chen, C.M. Ko, and B.A. Li, Phys. Rev. Lett. **94**, 032701 (2005) [arXiv:nucl-th/0407032].
[56] B.A. Li and L.W. Chen, Phys. Rev. C **72**, 064611 (2005).
[57] D. Shetty, S.J. Yennello and G.A. Souliotis, Phys. Rev. C **75,** 034602 (2007).
[58] T. Li et al., arXiv:0709.0567 [nucl-ex], Phys. Rev. Lett., (2007) (in press).
[59] P.J. Siemens, Nucl. Phys. **A141**, 225 (1970).
[60] O. Sjöberg, Nucl. Phys. **A222**, 161 (1974).
[61] I.E. Lagaris and V.R. Pandharipande, Nucl. Phys. **A369**, 470 (1981).
[62] F.S. Zhang and L.W. Chen, Chin. Phys. Lett. **18**, 142 (2001).
[63] A.W. Steiner, Phys. Rev. C **74**, 045808 (2006).
[64] B.A. Brown, Phys. Rev. Lett. **85**, 5296 (2000).
[65] S. Typel and B.A. Brown, Phys. Rev. C **64**, 027302 (2001).
[66] C.J. Horowitz, and J. Piekarewicz, Phys. Rev. Lett **86**, 5647 (2001); Phys. Rev. C **64**, 062802 (R) (2001); Phys. Rev. C **66**, 055803 (2002).
[67] R.J. Furnstahl, Nucl. Phys. **A706**, 85 (2002).
[68] S. Karataglidis, K. Amos, B.A. Brown, and P.K. Deb, Phys. Rev. C **65**, 044306 (2002).
[69] A.E.L. Dieperink, Y. Dewulf, D. Van Neck, M. Waroquier, and V. Rodin, Phys. Rev. C **68**, 064307 (2003).
[70] L.W. Chen, C.M. Ko, and B.A. Li, Phys. Rev. C **72**, 064309 (2005) [arXiv:nucl-th/0509009].
[71] A.W. Steiner and B.A. Li, Phys. Rev. C **72**, 041601(R) (2005).
[72] M. Prakash and K. S. Bedell, Phys. Rev. C **32**, 1118 (1985).
[73] M. Lopez-Quelle, S. Marcos, R. Niembro, A. Bouyssy, and N. V. Giai, Nucl. Phys. **A483**, 479 (1988).
[74] V. Baran, M. Colonna, M. Di Toro, V. Greco, and M. Zielinska-Pfabé, and H.H. Wolter, Nucl. Phys. **A703**, 603 (2002).
[75] M. M. Sharma et al., Phys. Rev. C **38**, 2562 (1988).
[76] B.G. Todd-Rutel and J. Piekarewicz, Phys. Rev. Lett. **95**, 122501 (2005).
[77] M. Jaminon, C. Mahaux, and P. Rochus, Phys. Rev. C **22**, 2027 (1980).
[78] M. Jaminon and C. Mahaux, Phys. Rev. C **40**, 354

(1989).
[79] H. Feldmeier and J. Lindner, Z. Phys. A **341**, 83 (1991).
[80] G.Q. Li and R. Machleidt, Phys. Rev. C **48**, 2707 (1993).
[81] P. Danielewicz, Nucl. Phys. **A673**, 375 (2000).
[82] S. Hama, B. C. Clark, E. D. Cooper, H. S. Sherif, and R. L. Mercer, Phys. Rev. C **41**, 2737 (1990).
[83] G.R. Satchler, Chapter 9: Isospin Dependence of Optical Model Potentials, in Isospin in Nuclear Physics, page 391-456, D.H. Wilkinson (Ed.), (North-Holland, Amsterdam, 1969).
[84] G.W. Hoffmann and W.R. Coker, Phys. Rev. Lett. **29**, 227 (1972).
[85] P.E. Hodgson, The Nucleon Optical Model, pages 613-651, (World Scientific, Singapore, 1994).
[86] A.J. Koning and J.P. Delarocje, Nucl. Phys. **A713**, 231 (2003).
[87] A.M. Lane, Nucl. Phys. **35**, 676 (1962).
[88] S. Fritsch, N. Kaiser and W. Weise, Nucl. Phys. **A750**, 259 (2005).
[89] L.W. Chen, C.M. Ko, and B.A. Li, Phys. Rev. C **72**, 064606 (2005) [arXiv:nucl-th/0508045].
[90] C.J. Horowitz, Phys. Rev. C **31**, 1340 (1985).
[91] D. P. Murdock and C. J. Horowitz, Phys. Rev. C **35**, 1442 (1987).
[92] Z.H. Li, L.W. Chen, C.M. Ko, B.A. Li, and H.R. Ma, Phys.Rev. C **74**, 044613 (2006).
[93] S. Typel, Phys.Rev. C **71**, 064301 (2005).
[94] T. Marketin, D. Vretenar, and P. Ring, Phys.Rev. C **75**, 024304 (2007).
[95] E. Chabanat, P. Bonche, P. Haensel, J. Meyer, and R. Schaeffer, Nucl. Phys. **A627**, 710 (1997).
[96] E. Chabanat, P. Bonche, P. Haensel, J. Meyer, and R. Schaeffer, Nucl. Phys. **A635**, 231 (1998).
[97] P.-G. Reinhard, Nucl. Phys. **A649**, 305c (1999).
[98] D. Lunney, J.M. Pearson, C. Thibault, Rev. Mod. Phys. **75**, 1021 (2003).
[99] H. Müller and B. D. Serot, Nucl. Phys. **A606**, 508 (1996).
[100] B. Liu, V. Greco, V. Baran, M. Colonna, and M. Di Toro, Phys. Rev. C **65**, 045201 (2002).
[101] S. Kubis and M. Kutschera, Phys. Lett. **B399**, 191 (1997).
[102] S.-J. Lee, J. Fink, A.B. Balantekin et al., Phys. Rev. Lett. **57**, 2916 (1986).
[103] G.A. Lalazissis, J. Konig, P. Ring, Phys. Rev. C **55**, 540 (1997).
[104] M.M. Sharma, M.A. Nagarajan, P. Ring, Phys. Lett. **B312**, 377 (1993).
[105] Y. Sugahara and H. Toki, Nucl. Phys. **A579**, 557 (1994).
[106] W.H. Long, J. Meng, N. Van Giai, S.G. Zhou, Phys. Rev. C **69**, 034319 (2004).
[107] J.K. Bunta and S. Gmuca, Phys. Rev. C **68**, 054318 (2003).
[108] T. Niksic, D. Vretenar, P. Finelli, P. Ring, Phys. Rev. C **66**, 024306 (2002).
[109] G.A. Lalazissis, T. Niksic, D. Vretenar, and P. Ring, Phys. Rev. C **71**, 024312 (2005).
[110] T. Klahn et al., Phys.Rev. C **74**, 035802 (2006).
[111] T. Gaitanos, M. Di Toro, S. Type, V. Baran, C. Fuchs, V. Greco, H.H. Wolter, Nucl. Phys. **A732**, 24 (2004).
[112] E.D. Cooper, S. Hama, B.C. Clark, and R.L. Mercer, Phys. Rev. C **47**, 297 (1993).
[113] H.F. Arellano, H.V. von Geramb, Phys. Rev. C **66**, 024602 (2002).
[114] C. Fuchs and H.H. Wolter, Eur. Phys. J. A **30**, 5 (2006).
[115] B. Liu, H. Guo, V. Greco, U. Lombardo, M. Di Toro, and Cai-Dian Lu, Eur. Phys. J. A **22**, 337 (2004).
[116] S.S. Avancini, D.P. Menezes, Phys. Rev. C **74**, 015201 (2006).
[117] W.Z. Jiang, B.A. Li, and L.W. Chen, Phys. Lett. **B653**, 184 (2007) [arXiv:0705.1738[nucl-th]].
[118] W.Z. Jiang, B.A. Li, and L.W. Chen, arXiv:0707.2795 [nucl-th].
[119] A. S. Khvorostukhin, V. D. Toneev, D.N. Voskresensky, Nucl. Phys. **A791**, 180 (2007).
[120] G. E. Brown, M. Rho, Phys. Rev. Lett. **66**, 2720 (1991).
[121] S. Typel, T. v. Chossy, and H. H.Wolter, Phys. Rev. C **67**, 034002 (2003).
[122] L.D. Miller, Phys. Rev. C **9**, 537 (1974).
[123] R. Brockmann, Phys. Rev. C **18**, 1510 (1978).
[124] M. Jaminon, C. Mahaux and P. Rochus, Nucl. Phys. **A365**, 371 (1981).
[125] C.J. Horowitz and B.D. Serot, Nucl. Phys. **A399**, 529 (1983).
[126] P. G. Blunden and M. J. Iqbal, Phys. Lett. **B196**, 295 (1987).
[127] A. Bouyssy, J.-F. Mathiot, N. Van Giai, and S. Marcos, Phys. Rev. C **36**, 380 (1987).
[128] P. Bernardos, V. N. Fomenko, Nguyen Van Giai, M. L. Quelle, S. Marcos, R. Niembro, and L. N. Savushkin, Phys. Rev. C **48**, 2665 (1993).
[129] R. Niembro, P. Bernardos, M. Lopez-Quelle, and S. Marcos, Phys. Rev. C **64**, 055802 (2001).
[130] S Marcos, L N Savushkin, V N Fomenko, M López-Quelle and R Niembro, J. Phys. G **30**, 703 (2004).
[131] M. Lopez-Quelle, L.N. Savushkin, S. Marcos, and R Niembro, J. Phys. G **30**, 703 (2004).
[132] W.H. Long, N. Van Giai, J. Meng, Phys. Lett. **B640**, 150 (2006).
[133] W.H. Long, H. Sagawa, J. Meng, N. Van Giai, Phys. Lett. **B639**, 242 (2006).
[134] W.H. Long, H. Sagawa, N. Van Giai, J. Meng, arXiv:0706.3497 [nucl-th].
[135] K. Weber, B. Blättel, W. Cassing, H.C. Dönges, V. Koch, A. Lang, and U. Mosel, Nucl. Phys. **A539**, 713 (1992).
[136] T. Maruyama, W. Cassing, U. Mosel, S. Teis, and K. Weber, Nucl. Phys. **A573**, 653 (1994).
[137] P.K. Sahu, W. Cassing, U. Mosel, A. Ohnishi, Nucl. Phys. **A672**, 376 (2000).
[138] B.A. Li, G.C. Yong and W. Zuo, Phys. Rev. C **71**, 014608 (2005).
[139] B.A. Li, G.C. Yong and W. Zuo, Phys. Rev. C **71**, 044604 (2005).
[140] B.A. Li, L.W. Chen, G.C. Yong, and W. Zuo, Phys. Lett. **B634**, 378 (2006).
[141] G.C. Yong, B.A. Li, L.W. Chen, and W. Zuo, Phys. Rev. C **73**, 034603 (2006).
[142] G.C. Yong, B.A. Li, L.W. Chen, Phys. Rev. C **74**, 064617 (2006).
[143] G.C. Yong, B.A. Li, and L.W. Chen, Phys. Lett. **B650**, 344 (2007).
[144] J. Xu, L.W. Chen, B.A. Li and H.R. Ma, Phys. Rev. C **75**, 014607 (2007).
[145] J. Xu, L.W. Chen, B.A. Li and H.R. Ma, Phys. Lett. **B650**, 348 (2007).